DISSERTAÇÃO DE MESTRADO Nº 978

ACTIVE DISTURBANCE REJECTION CONTROL APPLIED TO A TWIN-ROTOR SYSTEM

Jaime Arturo Dulce Galindo

DATA DA DEFESA: 07/04/2017

Universidade Federal de Minas Gerais

Escola de Engenharia

Programa de Pós-Graduação em Engenharia Elétrica

ACTIVE DISTURBANCE REJECTION CONTROL APPLIED TO A TWIN-ROTOR SYSTEM

Jaime Arturo Dulce Galindo

Dissertação de Mestrado submetida à Banca Examinadora designada pelo Colegiado do Programa de Pós-Graduação em Engenharia Elétrica da Escola de Engenharia da Universidade Federal de Minas Gerais, como requisito para obtenção do Título de Mestre em Engenharia Elétrica.

Orientador: Prof. Leonardo Antônio Borges Tôrres

Belo Horizonte - MG

Abril de 2017

Dulce Galindo, Jaime Arturo.
D881a Active disturbance rejection control applied to a twin-rotor system [manuscrito] / Jaime Arturo Dulce Galindo. – 2017.
xxiv, 75 f., enc.: il.

Orientador: Leonardo Antônio Borges Tôrres.
Coorientador: Guilherme Vianna Raffo.

Dissertação (mestrado) Universidade Federal de Minas Gerais, Escola de Engenharia.

Bibliografia: f. 69-75.

1. Engenharia elétrica - Teses. 2. Helicópteros - Teses. 3. Método de rastreio - Teses. 4. Rotores - Teses. I. Tôrres, Leonardo Antônio Borges. II. Raffo, Guilherme Vianna. III. Universidade Federal de Minas Gerais. Escola de Engenharia. IV. Título.

CDU: 621.3(043)

"Active Disturbance Rejection Control Applied to a Twin-rotor System"

Jaime Arturo Dulce Galindo

Dissertação de Mestrado submetida à Banca Examinadora designada pelo Colegiado do Programa de Pós-Graduação em Engenharia Elétrica da Escola de Engenharia da Universidade Federal de Minas Gerais, como requisito para obtenção do grau de Mestre em Engenharia Elétrica.

Aprovada em 07 de abril de 2017.

Por:

Prof. Dr. Leonardo Antônio Borges Tôrres
DELT (UFMG) - Orientador

Prof. Dr. Guilherme Vianna Raffo
DELT (UFMG) - Coorientador

Prof. Dr. Leonardo Amaral Mozelli
(UFMG)

Prof. Dr. Seleme Isaac Seleme Júnior
DELT (UFMG)

mαcrϕ@ufmg

Universidade Federal de Minas Gerais
Programa de Pós-Graduação em Engenharia Elétrica
Research group MACRO - Mechatronics, Control and Robotics

ACTIVE DISTURBANCE REJECTION CONTROL APPLIED TO A TWIN-ROTOR SYSTEM

Jaime Arturo Dulce Galindo

Belo Horizonte, Brazil
2017

Jaime Arturo Dulce Galindo

ACTIVE DISTURBANCE REJECTION CONTROL APPLIED TO A TWIN-ROTOR SYSTEM

Thesis submitted to the Graduate Program in Electrical Engineering of Escola de Engenharia at the Universidade Federal de Minas Gerais, in partial fulfillment of the requirements for the degree of Master in Electrical Engineering.

Advisor: Leonardo Antônio Borges Tôrres
Co-advisor: Guilherme Vianna Raffo

Belo Horizonte, Brazil
2017

To Hector Jaime, Elizabeth,
José Leonardo, Maria José,
and especially Teresa Quiroz.

Acknowledgements

During the course of my masters studies, several remarkable events happened in my life. Most of the experiences offerted by Brazilian people were good, although, inevitably, there are difficult times in life. However, my faith in God always kept me going on the true way, with my thoughts focused on "in the mount of the lord it shall be provided" (Genesis 22,1-19). Thereby, first of all, this achievement is dedicated to the almighty Lord. To whom I am very grateful for all the blessings, which are not coincidences of destiny.

I am very grateful to my advisor Leonardo Antônio Borges and my co-advisor Guilherme Vianna Raffo for the dedication support, orientation, patience, great comprehension before my sentences in *portuñol*, and for the friendship offered during my masters studies.

Thanks to the faculty of the UFMG that participated in my academic training, especially the professor Luis Antonio Aguirre for his teachings and orientations. Moreover, I would like to acknowledge the funding agencies FAPEMIG, CAPES and CNPQ for given me the opportunity to do my postgraduate studies in Brazil.

I would like to render thanks to all my friends of the MACRO and MACSIN laboratories: Brenner, Ernesto, Daniel, Frederico, Rafael, Letícia, Stella, Mariana, Ana, Marcelo, Diana, Freddy, Gabriela, Alex, Lucas, Petrus, Wendy and Marcus for participating in the "last question of day" (a subtle way to make several questions on the same day) and that were of paramount importance for the beginning and conclusion of this work.

I can not ignore the importance of my Colombian friends Diego Vicko, Edna, Karina, Marcela, Liliana and Brayan for accompanying me in this great adventure and for always remind me of my country.

Last, but not least, I would like to thank my father Hector Jaime Dulce for being my example and professional guide. To my mother Elizabeth Galindo for the unconditional support and for teaching me to act with intelligence in life. To my brother José Leonardo Dulce for motivating me to fight every day of my life. To my grandmother Teresa de Jesús Quiroz for motivating me with her courage and faith to deal with the difficulties of life. To the memory of my grandfather Fabio Galindo, who rest in the glory of God. To my stepbrother Juan Camilo Fonseca and my good friend Juan José Quiroz for the unconditional support during our master training, and to all my family and friends who have supported and enjoyed this achievement.

Agradecimientos

Durante el recorrido de mi maestría, un gran conjunto de historias trascendentales marcaron mi vida, de las cuales la mayoría fueron buenas experiencias ofrecidas por el acogedor pueblo brasileño y por otra parte, momentos difíciles que son inevitables en la vida. Sin embargo, mi fé en Dios me mantuvo siempre por el camino verdadero, pensando siempre que "En la montaña del Señor se proveerá" (Génesis 22,1-19). De modo que este logro es primeramente gracias al Señor, todo poderoso, a quien estoy agradecido por sus bendiciones, que no son coincidencias del destino.

Estoy muy agradecido con mi orientador Leonardo Antônio Borges y mi coorientador Guilherme Vianna Raffo, por la dedicación, apoyo, orientación, paciencia, gran comprensión ante mis frases en *portuñol* y la amistad brindada durante mis estudios de maestría.

Gracias al cuerpo docente de la UFMG que participó en mi formación académica, especialmente al profesor Luis Antonio Aguirre por sus enseñanzas y orientaciones. Además quiero agradecer a las agencias de financiamiento FAPEMIG, CAPES y CNPQ por permitirme la oportunidad de realizar mis estudios de postgraduación en brasil.

Quiero agradecer a todos mis amigos de laboratorio Brenner, Ernesto, Daniel, Frederico, Rafael, Leticia, Stella, Mariana, Ana, Marcelo, Diana, Freddy, Gabriela, Alex, Lucas, Petrus, Wendy, Marcus por participar de "la última pregunta del dia" (forma sutil de preguntar varias veces en el mismo dia) y que fueron de suma importancia para el inicio y conclusión de este trabajo.

No puedo pasar por alto los agradecimientos a mis amigos colombianos Diego, Vicko, Edna, Karina, Marcela, Liliana y Brayan por acompañarme en esta gran aventura y recordarme lo bueno que son las tradiciones Colombianas.

De ultimo, pero no menos importante, quiero agradecer a mi padre Hector Jaime Dulce por ser mi ejemplo y mi guía profesional. A mi madre Elizabeth Galindo por el apoyo incondicional y la enseñanza de actuar con inteligencia en la vida. A mi hermano José Leonardo Dulce por motivarme a luchar todos los días de mi vida. A mi abuelita Teresa de Jesús Quiroz por motivarme con su valentía y fé para afrontar las dificultades de la vida. A la memoria de mi abuelo Fabio Galindo quien descansa en la gloria de Dios. A mi hermanastro Juan Camilo Fonseca y mi buen amigo Juan José Quiroz por el apoyo incondicional durante nuestra formación como estudiantes de maestría, y a todos mis

familiares y amigos que me han apoyado y disfrutan de este logro.

Resumo

O problema de controle do sistema não-linear conhecido como Sistema Rotor-Duplo (TRS) usando a técnica de Controle por Rejeição Ativa de Distúrbios (ADRC) é investigado neste trabalho. O TRS é um equipamento comercial didático usado para estudar problemas de controle de helicópteros, tais como estabilização ou rastreamento de ângulos de arfagem e de guinada. Neste trabalho apenas um grau de liberdade é considerado, ou seja, o movimento do ângulo de arfagem do TRS, de modo que o TRS pode ser representado como um sistema de terceira ordem com uma entrada e uma saída (SISO). Os parâmetros do modelo fenomenológico para o TRS são obtidos minimizando o custo quadrático associado à diferença entre a resposta experimental e a resposta simulada. Como a saída do TRS é quantificada devido ao uso de um encoder rotacional, um Procedimento de Diferenciação Algébrica (ADP) é usado como uma técnica de filtragem para suavizar as transições bruscas causadas pela quantização. Além disso, uma estratégia de cancelamento parcial de dinâmica é utilizada para reduzir a ordem do sistema, considerando que a estratégia ADRC foi originalmente concebida para ser aplicada em sistemas de segunda ordem. Para alcançar esta redução de ordem, a derivada temporal de um sinal é estimada usando um Diferenciador Exato e Robusto (RED). Finalmente, a estratégia ADRC, modificada pela inclusão dos estágios de processamento de sinal providos pelo ADP e pelo RED, é testada através de experimentos com a plataforma TRS. Dados experimentais indicam desempenho superior em relação à formulação original do ADRC para o caso de rastreamento de referências desejadas do ângulo de arfagem.

Abstract

The problem of controlling the nonlinear system known as the Twin-Rotor System (TRS) using the Active Disturbance Rejection Control (ADRC) technique is investigated in this work. The TRS is a commercial didactical experiment that is used for studying helicopters' control tasks, such as pitch and yaw stabilization or tracking. In this work only one degree-of-freedom is considered, namely the TRS pitch movement, such that the TRS can be represented as a third order Single-Input Single-Output (SISO) nonlinear system. The parameters of a first-principles model are obtained by minimizing the quadratic cost associated with the difference between experimentally acquired response data and simulated ones. Since the TRS' output is quantized due to the use of a rotational encoder, an Algebraic Differentiation Procedure (ADP) is used as a filtering technique to smooth out the corresponding abrupt transitions caused by quantization. In addition, a partial dynamics cancellation scheme is employed to reduce the system order considering that the ADRC strategy was originally conceived to be applied in second-order systems. To accomplish this reduction, the time-derivative of a signal is estimated using a Robust and Exact Differentiator (RED) technique. Finally, the ADRC strategy, modified by the inclusion of signal processing stages provided by the ADP and the RED, is tested in practice. Experimental data indicates superior performance with respect to the original ADRC formulation in tracking a desired reference pitch angle.

Contents

List of Figures

List of Tables

Acronyms

ADP	Algebraic Differentiation Procedure
ADRC	Active Disturbance Rejection Control
BIBO	Bounded-Input Bounded-Output
DAC	Disturbance Accommodation Control
DOB	Disturbance Observer
DOBC	Disturbance Observer Control
DRC	Disturbance Rejection Control
ESO	Extended State Observer
FIR	Finite Impulse Response
FRD	Full Relative Degree
GPI	Generalized Proportional Integral
GPIO	Generalized Proportional Integral Observer
HGO	High Gain Observer
IADU	Integral of the Absolute Derivative of the Control signal
ID	Inverse Dynamics
iPID	Intelligent PID
ISE	Integral of the Squared Error
ITAE	Integral of the Time-weighted Absolute Error
MIMO	Multiple-Input Multiple-Output
PD	Proportional and Derivative

PID	Proportional Integrative and Derivative
RED	Robust and Exact Differentiator
SISO	Single-Input Single-Output
TPG	Transient Profile Generator
TRS	Twin-Rotor System
UFMG	Universidade Federal de Minas Gerais
UIO	Unknown Input Observer

List of Symbols

A_{ec}	Matrix used to choose the controller gains in the ADRC stability analysis.
$A_{\tilde{x}}$	Matrix used in the ADRC stability analysis.
A_{o}	Matrix used to choose the observer gains in the ESO convergence proof.
a	Coefficients of the polynomial time function of the ADP.
B_{o}	Constant matrix used in the ESO convergence proof.
b	Elements of the matrix A_{o}^{-1} used in the ESO convergence proof.
b_{f}	Viscous parameter in the joint of pitch.
C	Lipschitz constant.
$D(t)$	Time-derivative of the $F(t)$.
d	Elements of the matrix $e^{w_{\mathrm{o}}A_{\mathrm{o}}t}$ used in the ESO convergence proof.
e_{a}	Error computed by the ADRC.
e_{c}	Controller error.
e_{id}	Inverse dynamic error.
e_{id0}	Initial condition of the inverse dynamic error.
$F(t)$	Bounded nonlinear function that contains terms of the system's states.
$\hat{F}$	The extended state estimated by ESO.
$f(\tilde{x}, \beta, \varrho)$	Nonlinear function used in the nonlinear observer gains.
$G(t)$	Bounded nonlinear function.
$\hat{G}_{\mathrm{c}}$	Constant approximated to the bound of the nonlinear function $G(t)$.

$H[g,h]$	Space of measurable functions bounded on a segment $[g,h]$ defined for the RED.
I_{h}	Moment of inertia around the horizontal axis in the TRS.
I_{q}	Quantization interval.
J	The function cost employed to formulate the time-optimal solution.
j	Order of the time-derivative of the input signal used in the ADP kernel function.
K_{d}	Derivative controller gain.
K_{p}	Proportional controller gain.
k	Integer defined positive used in the ESO convergence proof.
k_{m}	DC motor static gain.
L	Observer gain vector of the nonlinear function.
L_{q}	Quantization levels.
ℓ	Observer gain vector.
M	Number of the integration steps in the ADP.
m_{g}	Parameter equal to the product of the weight force times to the distance from the center of mass to the center of the pitch axis revolute joint.
N	Order of the Taylor expansion used in the ADP kernel function.
n_{b}	Number of bits in the output quantization.
O	Elements of the matrix $e_{\mathrm{c}}^{A_{\mathrm{ec}}t}$ used in the ADRC stability analysis.
p	Part of the solution of the differential equation used in the ESO convergence proof.
p_{s}	Smoothing parameter.
r	Integer defined positive used in the ADRC stability analysis.
s	Laplace variable.
T	Time constant.
T_{adp}	Constant that represents the interval of integration in the ADP.
T_{f}	Torque associated to viscous friction in the joint of pitch.

T_{p}	Torque associated with the rotor's propulsion.
$T_{\mathrm{p}}^{\mathrm{d}}$	Desired propulsion torque computed by the ADRC.
T_{s}	Sample time.
T_{w}	Torque exerted by weight forces.
u	System's input.
u^*	Control signal of the time-optimal control problem.
u_{adrc}	ADRC control law.
u_{adrc}^*	Modified ADRC control in Zheng (2009).
u_{v}	Input voltage of the DC motor.
u_{vc}	Virtual control law of ADRC.
v	Constant used to limit $\lvert(A_{\mathrm{o}}^{-1}B_{\mathrm{o}})_i\rvert$ used in the ESO convergence proof.
$w(t)$	External disturbances.
w_{c}	Controller bandwidth.
w_{o}	Observer bandwidth.
x	State vector.
$\hat{x}$	Estimated states vector.
$\tilde{x}$	Observer error.
y	System's output.
y_{adp}	ADP output.
y_{r}	Measured pitch angle.
y_{ref}	Abrupt reference and the TPG input.
$y_{\mathrm{ref}}^{\mathrm{s}}$	State vector of the TPG and smooth reference vector.
y_{s}	Simulated output of the TRS model.
z	Switch function.
α_1, α_2	The propeller thrust coefficients.

α_{o}	Constants of the characteristic polynomial.
β	Rate of convergence velocity of the nonlinear function $f(\tilde{x}, \beta, \varrho)$.
γ	Constant used to limit the controller gains in the ADRC stability analysis.
δ	Constant used to limit nonlinear function $D(t)$ in the ESO convergence proof.
ζ	State vector of the double integrator system.
η	Constant used to limit $\lvert(A_{\text{o}}^{-1}e^{w_{\text{o}}A_{\text{o}}t}B_{\text{o}})_i\rvert$ used in the ESO convergence proof.
ϑ	Part of the solution of the differential equation used in the ADRC stability analysis.
κ	Parameter of the RED subsystem.
λ	Parameter of the RED subsystem.
μ	Output of the RED subsystem.
μ_1	State variable of the RED subsystem.
ν	Noise measurement associated with the quantization error and other effects.
φ	Pitch angle position of the TRS.
ξ	Variable transformation used in the ESO convergence proof.
$\Pi_{jN\varpi}$	ADP kernel function.
ϖ	An arbitrary nonnegative integer used in the ADP kernel function.
ϱ	Error limit to change of convergence velocity of the nonlinear function $f(\tilde{x}, \beta, \varrho)$.
ρ	Constant used to limit the controller error e_{c} in the ADRC stability analysis.
σ	Constant used to limit the observer error $\tilde{x}$ in the ESO convergence proof.
τ	Dummy variable in the ADP.
τ_{m}	Time constants of the DC motor.
χ	State variable of the RED subsystem.
Ψ	Vector used to solve the differential equation in the ADRC stability analysis.
ψ	Input signal of the RED subsystem.
ω	Rotational speed of the main rotor.

1 Introduction

1.1 Motivations

The model-free strategy called Active Disturbance Rejection Control (ADRC) has woken up great interest in automatic control area in the last few years. This fact involves the academia and industry sectors, where in the academia it is due to the interest of several journals of industrial control and control theory in publications related to disturbance rejection and rigorous mathematical definitions for ADRC, as shown in Chen et al. (2016). In the same way, according to Huang & Xue (2014), a part of the industrial sector has achieved improvements with the adoption of the ADRC strategy. It is the case of Parker Hannifin Extrusion plant in North America, that by using the ADRC strategy has obtained in over 50% energy saving per line across 10 production lines.

Nowadays, the attention of one part of the industrial sector dominated for the Proportional, Integrative and Derivative (PID) control has been captured by promising results from the ADRC. Unlike a traditional PID control, the function of a nonlinear controller is to manipulate a system with nonlinear dynamics in such a way that its control signal must compensate the system nonlinearities and force the system behavior to the requirements given by the reference. In this way, the ADRC is proposed with two complementary actions, the first one is to cancel the nonlinear dynamics of a determined group of nonlinear systems using a Disturbance Rejection Control (DRC) law, considering the system's nonlinearities as internal disturbances of the system; and the other action is used to control the resulting system with Proportional and Derivative (PD) controller (Gao, 2015).

Moreover, the dynamical cancellation of the ADRC also includes the active rejection of external disturbances. Therefore, the interesting ADRC idea is based on cancellation of the disturbances (internal and external) which rely on the estimation obtained from the Extended State Observer (ESO), in such way the nonlinear system (red line) behaves as a controlled linear system (blue line) as shown Figure 1.1.

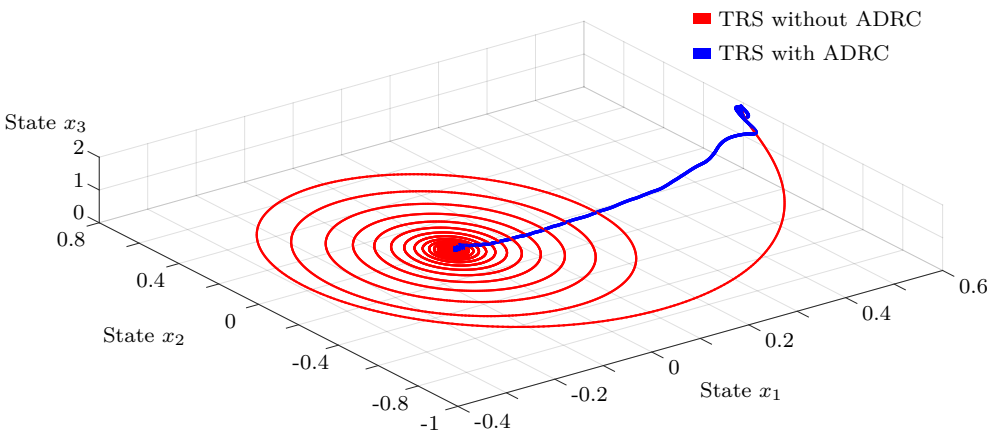

Figure 1.1: Behavior comparison between the nonlinear Twin-Rotor system (TRS) and the nonlinear TRS controlled with the ADRC; using the information given by the time-evolution of the TRS states.

The design of controllers for nonlinear dynamic systems usually relies on specific strategies for specific classes of systems, with these classes defined by properties associated with the underlying mathematical models of the systems under consideration (Slotine & Li, 1990; Khalil, 2001). Contrary to this well-established approach of investigating, the control problem in rigorous mathematical ground based on well-defined mathematical model, recently some very interesting works have been published defending the opposite idea of using "model-free" strategies to control the nonlinear systems. Particularly, one can highlight the influential work by the professor[1] Han (2009) shown in Figure 1.2, where a new universal control strategy, known as ADRC, is purposely designed as a replacement for the popular PID controller. In the same vein, Fliess & Join (2013) have presented the idea of using time-derivatives estimations as a step in order to control the nonlinear systems without knowing the underlaying mathematical model.

The common point between these two model-free strategies can be seen as the attempt to cancel the original dynamics of the system by means of an appropriate estimation of high-order time-derivatives of the system's output. This means that the presence of abrupt changes in the output signal, as it would be expected if the system's output is quantized, could be deleterious to the performance of the closed-loop system. In the same way, this issue has affected for a long time the control design with speed estimation. Usually, this

[1]Deceased in April, 2008. See from the message made by Bogdan M. Wilamowski, Editor-in-Chief of IEEE Transactions on Industrial Electronics, in Han (2009).

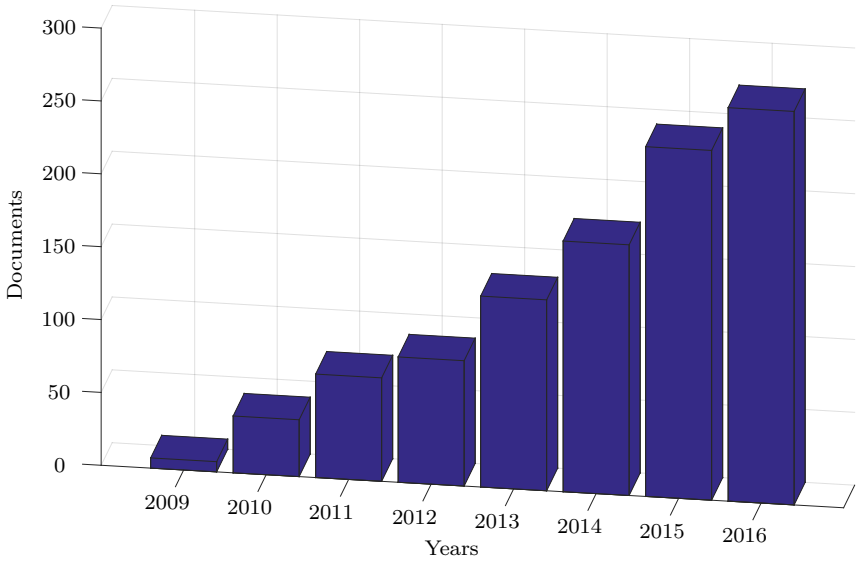

Figure 1.2: Citations of the ADRC paper (Han, 2009) (Source: Scopus).

problematic requires a hard study in observer models in order to improve the control performance and reduce the output quantization effect (Vivas Venegas, 2004).

On the other hand, the aerospace industry is one of the industrial sector interested in the use of controllers for nonlinear systems (López-Martínez, 2005). Due to the nature described by the actuators of an aircraft and its flight dynamics, the aircrafts are considered as nonlinear systems. As commented before, the advantages of using a nonlinear control are: the good behavior resulting from the system due to the suitable control signal computed, and a decrease in the response time of the system. This advantages are desired for the control of an aircraft. Moreover, due to the aerodynamic forces and the parametric uncertainties an additional requirement of an aircraft's controller is to be robust against this type of disturbances.

Helicopter control is a complex issue in aerospace industry, due to nonlinearities from its dynamics and the strong cross coupling of the actuators. According to Le et al. (2013), the Twin-Rotor System (TRS) is an electromechanical prototype that could represent a helicopter with fewer degrees-of-freedom. However, the propulsion mechanisms of both systems are different. The helicopter can change the propeller blade angle of attack to variate the propulsion, while the TRS propeller blades have a fixed angle of attack. Thus, it can vary the propulsion only with the rotational speed of its rotors that depends on the input voltage. Thereby, the only control inputs of the TRS are the voltages applied to the DC motors to regulate their rotational speed, which produce reaction forces and consequently a dynamic coupling in the TRS.

1.2 Overview

This section presents a literature review for disturbance estimator based control and the active disturbance rejection control.

1.2.1 Disturbance estimators based control

A survey of disturbance estimators has been published in a special issue in the last few decades. Contrary to state observers proposed by the modern control theory based on rigorous models and applied in feedback control or fault detection (Gertler, 1988), the disturbance estimators are based only on input-output data of the system, and they are used to complement control problems for systems with significant disturbances and parametric uncertainties (Radke & Gao, 2006). Taking into account this advantage, the controllers based on disturbance estimators have woken up great interest in the industrial society and have been applied in several sectors such as: mechatronics systems, chemical and process system, aerospace system, among others (Chen et al., 2016).

Unknown Input Observer (UIO) was one of the first disturbance estimators, which was proposed by Johnson (1968), where a state observer is formulated with an additional stated augmented to estimate disturbances. In this publication the UIO is used in a linear regulation optimal control problem with constant external disturbance. Later in Johnson (1970), the UIO formulation is generalized to accommodate the case of unmeasurable disturbances satisfying a linear differential equation. In Johnson (1971), the regulator and servomechanism theories are modified based on UIO, considering the presence of persistent fluctuating disturbances. Thereafter, the control strategy based on the UIO is formally presented as Disturbance Accommodation Control (DAC) in Mohadjer & Johnson (1983), where it is applied in load frequency control of an interconnected power system. In Johnson (1985) the DAC formulation is extended to include the case of internal disturbances arising from uncertain plant-parameters variations. An interesting unifying view of the existing disturbance decoupling observer is proposed in Takahashi & Peres (1999), where different approaches of linear algebraic and geometric design methods and variable structure/sliding modes methods are put together into a single framework. A survey of the DAC research line is shown in Johnson (2008), where the origin, evolution and the active study of real-time disturbance-observers are corroborated.

Another kind of disturbance estimator is the Disturbance Observer (DOB) proposed by Ohishi et al. (1983), which under the assumption that in plants of minimal phase the observer can estimate the disturbances using the inverse nominal transfer function of the plant. One of the first applications of DOB was proposed in Umeno & Hori (1991), where a good performance of the robust speed control system for DC servomotors is achieved based on parametrization of two degrees-of-freedom controllers with a microprocessor relying on DOB. Later in Lee & Tomizuka (1996), the DOB is used again to compensate the

external disturbances and the plant uncertainties in a robust feedback controller, which is part of an interesting controller structure for robust high-speed and high-accuracy motion control systems. The nonlinear extension of DOB is proposed in Chen et al. (2000), where it was applied in robot manipulators for compensating the friction and indicating that it can be also used for various purposes such as independent joint control, sensorless torque control and fault diagnosis in robots. A new extension of the PID controller together with the DOB is proposed by Schrijver & Van Dijk (2002). In this work, it is shown that a disturbance observer can be transformed into a classical feedback structure, which is applied for a rigid robot manipulator and is compared with a passivity based controller. Thereafter, the control strategy for nonlinear system based on DOB is formally presented as Disturbance Observer Control (DOBC) in Chen (2004). The research line of DOB remains active in the search of new analysis and design tools for DOBC as shown in Sariyildiz & Ohnishi (2013).

The High Gain Observer (HGO) when used in a feedback control loop, can be regarded as an estimator of disturbances due to its disturbance rejection capability and robustness to system uncertainties. The HGO was used for the first time with a linear control in Doyle & Stein (1979), where it is used to recover the frequency-domain properties achieved by a state feedback. Thereafter, the utility of the HGO was extended to nonlinear feedback control system as shown in Khalil & Saberi (1987); Saberi & Sannuti (1990); Tornambe (1989). In 1992, two papers were published, which carried out the beginning of two research schools of the HGO. One research line is represented by Gauthier et al. (1992), whose research is focused on cover a wide class of nonlinear systems and obtain the global results under global growth conditions. The other one is represented by Esfandiari & Khalil (1992), whose research is focused on the peaking phenomenon, which is an important feature of the HGO. In Khalil (2001) the HGO formulation is explained in detail. The HGO research line remains active proposing some alternatives to solve the peaking phenomenon and the measurement noise in the HGO, as shown in Khalil & Praly (2014) and Khalil & Priess (2016), respectively.

Similar to disturbance observer based control, a recent control strategy based on time-derivative estimation has been developed. The common point of both control strategies is the disturbance rejection ability and good performances attained with parametric uncertainties using only the input-output data of the system. The time-derivative estimation relies on algebraic methods, it is known as Algebraic Differentiator Procedure (ADP). One of the first implementation of the ADP was in the parametric identification of linear system in Fliess & Sira-Ramírez (2003). This approach showed good robustness properties with respect to a larger variety of additive disturbances. Later in Fliess & Sira-Ramírez (2004), the state estimation provided by the ADP was extended to nonlinear system and used for state feedback control around the flatness-based reference trajectory. In addition, Fliess & Join (2008) proposed a new control strategy, known as Intelligent PID controllers (iPIDs),

which is used for plants with unknown part that can be highly nonlinear or time-varying. A survey of the ADP is presented in Mboup et al. (2009), where the algebraic method is explained and implemented as a Finite Impulse Response (FIR) digital filter. The research line of the ADP based iPID controllers remains active in the implementation of several numerical simulations. Besides, it is presented as a model-free control in Fliess & Join (2013).

Another recent disturbance observer is the Generalized Proportional Integral Observer (GPIO), which is based on a linear configuration that includes an internal model relying on time polynomials approach to estimate the system's internal and external disturbances. One of the first applications of the GPIO was in the robust Generalized Proportional Integral (GPI) controller for trajectory tracking of induction motor in Cortés-Romero et al. (2009), where the obtained results showed a robustness of the control strategy against unknown load torque disturbance inputs, parametric uncertainties, and high frequency measurement noises. Among interesting applications of the GPI control, the problem of synchronization of chaotic oscillator in Luviano-Juarez et al. (2010), and the control problem of a buck converter with uncertain load in Sira-Ramírez et al. (2010) are dealt. The research line of the GPIO based control remains active in the application of several experiments as shown in Sira-Ramírez et al. (2011), where the GPI control is considered as a robust linear control for flatness nonlinear systems.

This work is focused on the disturbance estimator known Extended State Observer (ESO), which is studied in depth with the active disturbance rejection control in Section 1.2.2.

1.2.2 Active disturbance rejection control

According to Xue & Huang (2011) the active disturbance rejection control is a disturbance estimator based control, which is regarded as a breakthrough in the research of controlling uncertain systems due to its skill of controlling nonlinear systems with mixed uncertainties. The ADRC's disturbance estimator is known as ESO, which is a nonlinear observer that contains an additional state to estimate the internal and external disturbances of the nonlinear systems. The ESO and ADRC ideas arose from the control research of the Chinese professor Jingqing Han, who started his first publications in Han (1989; 1995; 2008, *apud* Gao (2015)), which were written in Chinese. Later, the ADRC began to be known with the English publications proposed by the professor Zhinqiang Gao and et al. (Gao et al., 2001; Gao, 2006; Sun, 2007; Yoo et al., 2007). One of the most representative works of the ADRC was published in Han (2009), which is used as a reference to show the ADRC strategy.

Some works have been proposed in order to define the ADRC strategy from a more rigorous point of view in control theory. In Gao (2006), the ADRC control stability is

analyzed for a linear system with external disturbance; in Zheng et al. (2007, *apud* Zheng (2009)), the ADRC control stability is evaluated for nonlinear system assuming that the nonlinearities are bounded; and recently, in Li et al. (2016), the local stability of the ADRC strategy applied to a nonlinear system was formally proved. In spite of these works, the stability prove for the ADRC control continues to be an active issue research.

A benchmark of the ADRC strategy applied in a motion control platform is given in Tian & Gao (2009), which shows that ADRC can be a viable replacement of the existing industry controllers in manufacturing due to the wide range of performance improvement achieved by ADRC. Moreover, the ADRC has been implemented in complex systems such as the Steward platform (Su et al., 2004); permanent-magnet synchronous motors (Su et al., 2005), DSP design for 1-kW H-bridge DC-DC power converter (Sun & Gao, 2005); cross coupled aerodynamic system (Madoński & Herman, 2011); extrusion process (Zheng & Gao, 2012); vibration suppression in two-inertia systems (Zhao & Gao, 2013); robotic-enhanced limb rehabilitation trainings (Madoński et al., 2014); variable geometry turbine and exhausting gas circulation system of diesel engines (Xie et al., 2016), among others. The obtained results in these experiments showed robustness with respect to parametric uncertainties, disturbance rejection capabilities, energy saving, good performance, and flexibility of the ADRC strategy.

As aforementioned, the ADRC strategy has been widely used in many different systems, where experimental results showed good performance. However, sometimes the ADRC structure has been modified to deal with some specific requirements of the systems. One of the first modified ADRC was proposed by Zheng & Gao (2014), where a predictive structure in the ADRC is used to compensate the control action for systems with time-delay. The simulation results obtained showed that the predictive ADRC strategy dealt with the time-delay of the process. In Madoński et al. (2015), an additional structure is proposed to estimate the critical gain parameter used in the ADRC control law. The results obtained by this modified ADRC in a simulation case study showed a performance improvement over the classic ADRC. Another modified ADRC for time-delay systems is proposed by Zheng & Gao (2016), where an equivalent structure is used to compensate the time-delay of the system's input data in the ESO. The performance improvement achieved by this modified ADRC is corroborated in simulation results. The research line of the ADRC strategy remains active in the mathematical study of ADRC stability, improvements of the ADRC structure, and new applications of the ADRC.

1.3 Problem statement

As commented in the previous section, the ADRC strategy is very interesting to control industrial process and benchmark systems, but due to some requirements of systems with nonlinear dynamics, parametric uncertainties, and high frequency noise in the system's

measurements, the ADRC has been modified. The modifications of the ADRC strategy to deal with nonlinear dynamical systems presenting quantized output and relative degree higher than two have not been well addressed in the literature. It only has been proposed an ADRC that uses the extension of time-derivative estimation of the reference (Zheng, 2009).

Twin-rotor system is used in this work to evaluate the control performance of the ADRC through simulation and experimental tests. The TRS is controlled to track a time-varying reference in pitch motion considering blocked the yaw movement around the vertical axis. In this way, the ADRC must deal with the nonlinear dynamics and the external disturbances of the TRS.

The system's quantized output is an effect derived from the sensor resolution used in the system. For the case of the TRS, due to the resolution of the incremental encoder used to measure the pitch motion, the system's output is quantized. The ESO included in the ADRC strategy is a disturbance observer, whose estimation is affected by the high frequency noises present in the system's output measure. Thereby, the ADRC may present difficulty controlling the TRS. This thesis contributes with an alternative solution to deal with the motor dynamics and output quantized issues from TRS, proposing a modified ADRC that includes an inverse dynamic and an algebraic differentiator procedure.

1.4 Objectives

The main objective of this thesis is to contribute to the development and implementation of the modified ADRC strategy for solving the tracking problem on pitch motion of the TRS. For the fulfillment of the main objective it is proposed three specific objectives, which are organized as follows:

- Development of the TRS model in pitch motion described in state equations and validation of the model using the measurements from the real TRS.
- Synthesize the ADRC strategy for the TRS and evaluate the control performance considering the tracking error and power consumption in simulation and experimental tests.
- Design modified ADRC models for the TRS and evaluate the control performance considering the tracking error and power consumption in simulation and experimental tests.

1.5 Thesis structure

This theses is organized as follows:

- **Chapter 2** describes the equations of pitch motion of the TRS using the Newton's second law. The nonlinear representation of the TRS in state equation is achieved including its quantized output. The parameter identification and model validation are performed using measurements of the pitch angle obtained from the real TRS.

- **Chapter 3** presents the ADRC strategy and the system's assumptions used for its formulation. The main ADRC components are described and the stability prove is presented together with its assumptions.

- **Chapter 4** designs the modified ADRC strategy, describing the new elements added to the ADRC. Simulation results of the TRS with two pure ADRC and two modified ADRC strategies are presented.

- **Chapter 5** presents the experiment setup and the test description followed by the results obtained in the real TRS with two pure ADRC and two modified ADRC strategies.

- **Chapter 6** summarizes the content and the main contributions of this thesis, and presents the future works of this research line.

2

Twin Rotor System Mathematical Modeling

In this chapter, we are going to present the mathematical model and the main characteristic of the twin-rotor system (TRS).

This chapter is organized as follows: Section 2.1 presents the twin-rotor system; Section 2.2 shows the dynamical model of the TRS in pitch motion; Section 2.2.1 describes the weight force model; Section 2.2.2 describes the friction model considered by TRS; Section 2.2.3 describes the actuator model; Section 2.3 explains the output quantization of the TRS; and finally, Section 2.4 describes the parameters estimation and shows the validation model.

2.1 The Twin Rotor System

The TRS is an electromechanical system with two-degrees of freedom associated with the pitch and yaw movements as illustrated in Figure 2.1. This system is used in didactic control experiments and it was manufactured by the *Feedback Instruments Ltd.*. By the time this monograph was written, one unit of the TRS was available to experimentations in the Control Laboratory of the Department of Electrical Engineering at UFMG.

The TRS has two rotors with caged propellers that are connected by a rod, and two angular position sensors, such that each pair rotor-sensor is associated with one of the possible pitch and yaw movements. Both rotors are actuated by DC brushless motors, whose angular velocity is controlled by varying the applied input voltage. The angular movements of the system are performed mainly by torques resulting from the propulsive

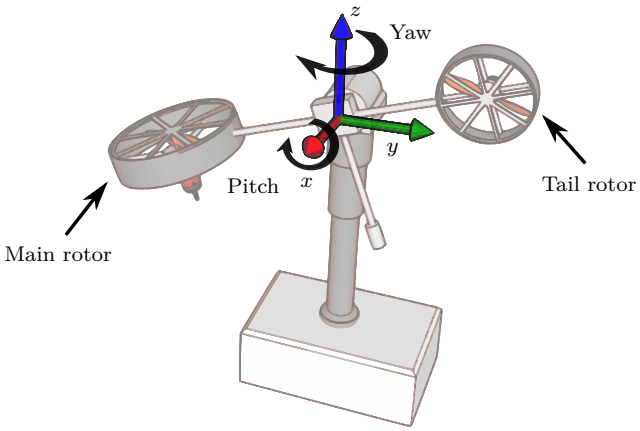

Figure 2.1: Twin-Rotor System – TRS.

forces generated by the propellers rotational speed. The angular position sensors are incremental encoders with limited resolution, which are located at the revolute joints that allow the pitch and yaw movements of the system.

By locking up the yaw movement around the vertical axis, the rod that connects the two propellers is allowed to swing up and down as it changes the pitch angle orientation around the horizontal axis, and the TRS becomes an one-degree of freedom mechanism, as shown in Figure 2.2. Therefore, the TRS considered in this work is composed mainly of the propulsive torque associated with the rotational speed ω, which depends on the input voltage u_{v} applied to the main rotor DC brushless motor, and the pitch angle position φ, measured by its respective incremental encoder, as is shown in Figure 2.2.

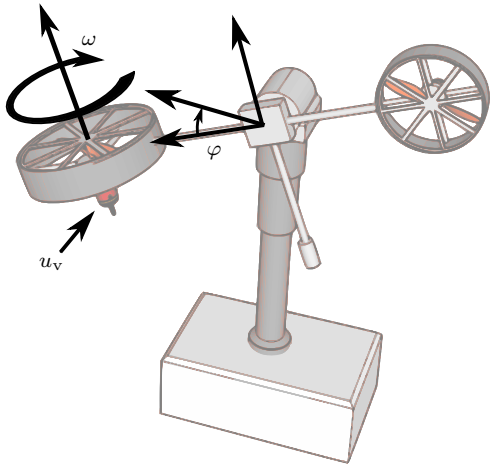

Figure 2.2: One-degree of freedom Twin-Rotor System with variable pitch attitude.

2.2 Dynamical Modeling: Equations of Motions

The dynamical model of the TRS can be formulated through the application of Newton's second law, in which all torques that determine the rotational movement around the

horizontal axis are summed up to comprise the final torque acting on the system. This approach follows the derivation presented in Feedback (2006). Among the individual contributions to the resulting torque we consider the torque T_{w} exerted by weight forces, the torque T_{f} due to viscous friction in the joint of pitch movement, and the torque T_{p} associated with the rotor's propulsion, which are summed as follows

$$I_{\mathrm{h}}\ddot{\varphi} = T_{\mathrm{p}} - T_{\mathrm{w}} - T_{\mathrm{f}}, \tag{2.1}$$

where $\ddot{\varphi}$ is the pitch acceleration, and I_{h} is the Twin-Rotor moment of inertia around the horizontal axis.

A state-space representation of the TRS model (2.1) can be obtained using the state variables $x_1 = \varphi$ and $x_2 = \dot{\varphi}$

$$\begin{aligned} \dot{x}_1 &= x_2, \\ I_{\mathrm{h}}\dot{x}_2 &= T_{\mathrm{p}}(\omega) - T_{\mathrm{w}}(x_1) - T_{\mathrm{f}}(x_2), \end{aligned} \tag{2.2}$$

where T_{p} is related to the system's input u_{v} – the DC voltage applied to the brushless motor – which depends on the rotational speed ω of the propeller, as it will be detailed in Section 2.2.3. The dependence of the remaining torques on the state variables is detailed in the next sections.

2.2.1 Weight Force Model

The TRS mechanical design is such that the center of gravity does not coincide with the center of rotation, hence there is a weight force restoration effect that leads the mechanism to an equilibrium point that corresponds to a nonzero inclination with respect to the horizontal direction when there is no additional applied torque. This torque is given by

$$T_{\mathrm{w}}(x_1) = m_{\mathrm{g}} \sin(x_1), \tag{2.3}$$

with $m_{\mathrm{g}} > 0$, a parameter equal to the product of the weight force times to the distance from the center of mass to the center of the pitch axis revolute joint.

2.2.2 Friction Model

In the literature we can find different friction models according to their mathematical complexity, like *Viscous Plus Coulomb Memoryless Model*, *Armstrong Model* and *LuGre Model* (Kelly et al., 2000). The friction model used in the TRS modeling developed in Feedback (2006) was formulated employing *Viscous Plus Coulomb Memoryless Model*, such

as

$$T_{\mathrm{f}}(x_2) = b_{\mathrm{f}} x_2 + b_{\mathrm{f2}} \mathrm{sign}(x_2),$$

where $b_{\mathrm{f}} > 0$ is the viscous parameter, and $b_{\mathrm{f2}} > 0$ is the Coulomb parameter.

We use a simplified friction model in this work, accounting only for the viscous damping, which is a differentiable function of the pitch speed x_2 given by

$$T_{\mathrm{f}}(x_2) = b_{\mathrm{f}} x_2. \tag{2.4}$$

In this work, effects from Coulomb friction are regarded as unknown disturbances.

2.2.3 Actuator Model

As implicitly shown in (2.2), the propulsion torque is associated with the rotational speed ω of the main rotor propeller.

Propulsion torque models can be computed using a quadratic expression of rotational speed ω, which is used by Feedback (2006) and given by

$$T_{\mathrm{p}} = \alpha_1 \omega^2 + \alpha_2 \omega, \tag{2.5}$$

where $\alpha_1 > 0$ and $\alpha_2 > 0$ are the propeller thrust coefficients of the quadratic and linear terms respectively.

Considering the voltage u_{v} applied to the brushless DC motor as the system's input that drives the propeller, we must represent the relation between u_{v} and ω. The DC motor model used in this work is a simplified one that represents the DC motor dynamics as a first-order linear system, neglecting the DC motor armature electrical current dynamics (Fitzgerald et al., 2003), which is given by

$$\tau_{\mathrm{m}} \frac{d\omega}{dt} = -\omega + k_{\mathrm{m}} u_{\mathrm{v}}, \tag{2.6}$$

where ω is the propeller's output rotational speed; u_{v} is the system's applied input voltage; τ_{m} is a time constant; and k_{m} is the DC motor static gain. The actuator model of the TRS combining (2.5) and (2.6) follows the same structure proposed in Feedback (2006) and it can be represented by the block diagram in Figure 2.3.

2.3 Output Quantization

Quantization of the system's output signal introduces high frequency content associated with abrupt changes in the measured values. This quantization error in the system's output is an issue for the control area, because it affects the process of estimating the

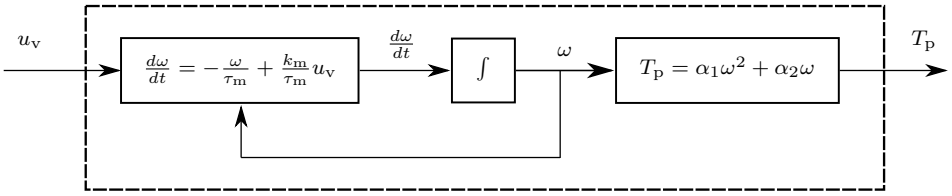

Figure 2.3: Actuator model.

state vector by relying on an observer, when the controller does not have full access to all system's states.

An example of the effect of output quantization in the estimation of the angular speed and acceleration from shaft encoder measurements is shown in Tilli & Montanari (2001). It is assumed that rarely the velocity is measured using a tachogenerator in a system with position/speed controller, hence it is necessary to estimate the speed in some way using the position measurement with quantization error.

Error quantization and external disturbances present in the output measurement are also subjects of interest in recently published works in the context of nonlinear high-gain observers (Prasov & Khalil, 2013) and robust nonlinear observers (Shim & Liberzon, 2016).

Quantization in the TRS is a consequence of using an incremental encoder to measure the pitch angle, which has limited resolution, leading to quantization of system's output as is shown in Figure 2.4.

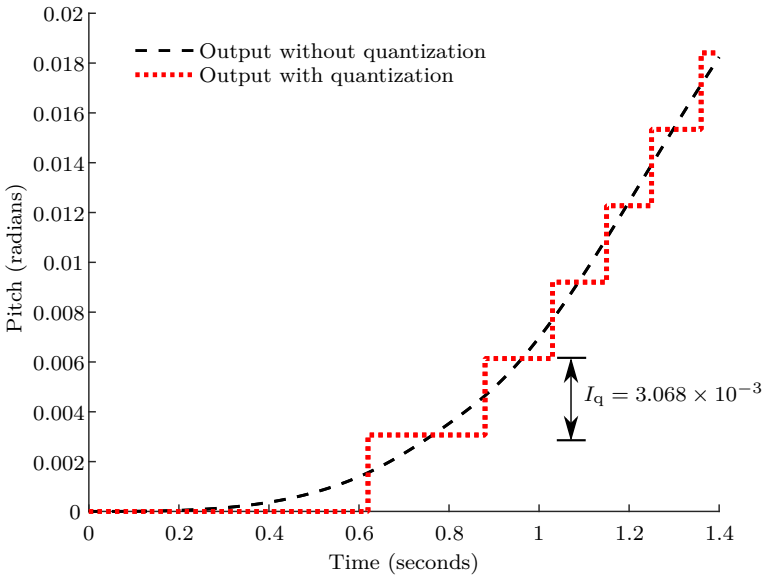

Figure 2.4: TRS system output quantization due to the incremental encoder.

Experimentally we have found a quantization interval I_q equal to 3.068×10^{-3} radians. Additionally, we can compute the number of bits used in the quantization of the output using the difference between φ_{max} and φ_{min} measurements of the pitch angle, and by dividing

this value by the quantization interval,

$$L_{\mathrm{q}} = \frac{\varphi_{\max} - \varphi_{\min}}{I_{\mathrm{q}}} = \frac{1.57}{3.068 \times 10^{-3}} = 511.73 \approx 512.$$

Since the number of quantization levels $L_{\mathrm{q}} = 2^{n_{\mathrm{b}}}$, where n_{b} is the number of bits $n_{\mathrm{b}} = 9$.

2.4 Parameters Estimation and Model Validation

For the parameters estimation of the TRS model it was considered a state-space system including the equations (2.3), (2.4), (2.5) and the actuator model (2.6). Hence, the TRS state-space model from (2.2) is augmented with one additional differential equation such that it becomes a third order system described by

$$\begin{aligned} \dot{x}_1 &= x_2, \\ I_{\mathrm{h}}\dot{x}_2 &= \alpha_1 {x_3}^2 + \alpha_2 x_3 - m_{\mathrm{g}} \sin(x_1) - b_{\mathrm{f}} x_2, \\ \tau_{\mathrm{m}}\dot{x}_3 &= -x_3 + k_{\mathrm{m}} u_{\mathrm{v}}, \\ y &= x_1 + \nu \end{aligned} \tag{2.7}$$

where $x_1 = \varphi$ is the pitch angle; $x_2 = \dot{\varphi}$ is the pitch angular speed; $x_3 = \omega$ is the rotational speed of the main rotor propeller; u_{v} is the DC motor input voltage; and y is the output measurement perturbed by the noise measurement ν associated with the quantization error and other effects.

By minimizing the mean square error between the *measured* pitch angle y_{r} and the *simulated* output y_{s} of the TRS model, while using the same input signal as shown in Figure 2.5, the set of parameters I_{h}, α_1, α_2, m_{g}, b_{f}, τ_{m} and k_{m} was obtained. In the literature, the TRS parameters identification is achieved in a similar way through an optimization technique shown in Rotondo et al. (2013) and Gorczyca et al. (2013).

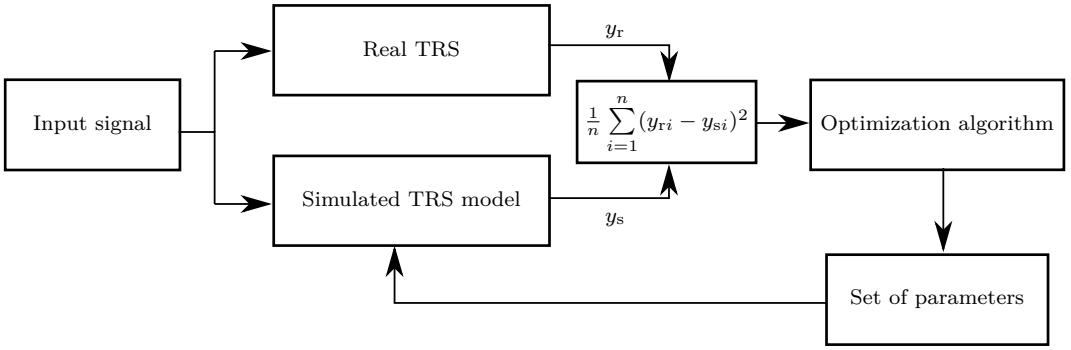

Figure 2.5: Parameters optimization.

To carry out the estimation process of the TRS parameters, we have made use of an interior-point algorithm whose initial condition for the parameters was chosen to be equal

to the nominal values described in Feedback (2006). The integration method used for simulating the TRS model was the fixed-step 4th order Runge-Kutta algorithm (Davis & Rabinowitz, 2007) with integration time of 0.01 seconds and a simulation time of 100 seconds.

To better analyzed the TRS nonlinear dynamics, seven different input signals were employed. For each input signal profile, the optimization process of minimizing the mean square error led to a corresponding set of parameters, as shown in Table 2.1. Figure 2.6 illustrates the process response for an input signal comprised by abrupt changes in the DC motor input voltage, which was obtained for the third excitation signal employed in these identification procedure.

Parameters identification	
Optimal set	Error indexes
Set 1	3
Set 2	2.9
Set 3	3
Set 4	1.9
Set 5	3.3
Set 6	0.78
Set 7	1.3

Table 2.1: Error indexes (multiplied by a factor 1×10^3) for each optimized set of parameters obtained using each input signal, respectively.

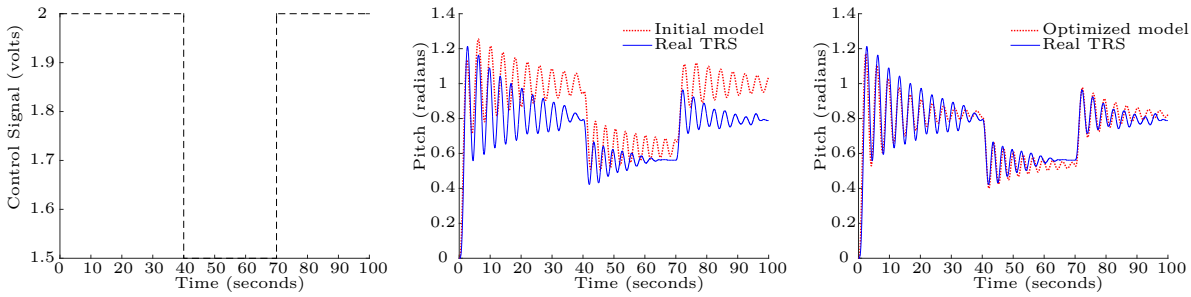

(a) Input signal. (b) Initial model. (c) Optimized model.

Figure 2.6: TRS model identification process for one particular type of excitation.

To select the best set of parameters among the seven sets obtained using different input signals, a cross-validation process (Aguirre, 2004) was implemented.

The validation was based on the evaluation of the error between the experimental data and the model outputs generated in the following way. The set of parameters associated with a specific type of input was used in the TRS model, and all 6 input signals not used to obtain this particular set of parameters were applied to the model. The corresponding 6 simulated outputs were then compared with the associated experimental data for each type of input signal. This comparison was quantified by integrating the square value of

the errors between the simulated output and the associated experimental output and, finally, by summing up all the 6 values, one for each type of input signal profile, as shown in Table 2.2.

Parameters validation								
Optimal set	I.S. 1	I.S. 2	I.S. 3	I.S. 4	I.S. 5	I.S. 6	I.S. 7	Total
Set 1	–	11.6	30.1	$*$	17	13.7	$*$	$*$
Set 2	8	–	6.3	8.7	5.8	2.1	5.6	36.5
Set 3	10.2	6.0	–	3.4	7	1.6	2.3	30.5
Set 4	9.7	7.5	3.9	–	11.3	1.3	1.4	35.1
Set 5	7.9	5.1	5.9	16.3	–	2.5	11.6	49.3
Set 6	9.3	9	4.8	3.9	10	–	2.6	39.6
Set 7	10.4	8.2	4.4	2.0	12.2	1.4	–	38.6

I.S. Input signal.

$*$ infinite value due to unbound response of model.

Table 2.2: Error indexes (multiplied by a factor 1×10^3) for the TRS identified model cross-validation.

From Table 2.2 it is concluded that the set 3 is the best selection due to the smallest resulting error index. Also, it is important to note that due to the fact that the TRS model does not consider the limit of the pitch motion, some unbounded response were obtained for the set 1 of parameters.

In Table 2.3 the set 3 of parameters are presented.

Parameter	Value
m_{g}	$0.3199\,\mathrm{Nm}$
I_{h}	$7.02 \times 10^{-2}\,\mathrm{kg\,m^2}$
α_1	$0.0152\,\mathrm{Nm/(rad/s)^2}$
α_2	$0.0738\,\mathrm{Nm/(rad/s)}$
b_{f}	$11.5 \times 10^{-3}\,\mathrm{Nms/rad}$
τ_{m}	$0.7185\,\mathrm{s}$
k_{m}	$1.0965\,\mathrm{(rad/s)/V}$

Table 2.3: Identified TRS parameters.

2.5 Final Remarks

This chapter presented the mathematical model of the TRS configured with an one-degree of freedom associated with pitch motion. The weight forces, the viscous friction and the propulsion torques present in the rotational movement around the horizontal axis are considered to describe the TRS in a second-order state-space model, which has as input signal the propulsion torque, which will be used in Chapter 4.

The models of weight forces, viscous fiction model and the propulsion torque including the DC motor model are put together with the quantization error of the system's output in order to rewrite the TRS model as a third-order state-space representation, which will be used in Chapters 4 and 5.

After obtaining the TRS model, a parameter identification was carried out using seven input signals profiles and the minimization of the mean square error between the measured pitch angle of the TRS and the simulated output of the TRS model. From the parameter identification, seven sets of TRS parameters were obtained, among which the set with the smallest resulting error index was chosen from a cross-validation. This set of the TRS parameters is used to design the modified ADRC in Chapters 4 and 5.

3

Active Disturbance Rejection Control

The Active Disturbance Rejection Control (ADRC) is the result of a research carried out by professor Han (2009). This strategy is based on the formulation of a feedback control, especially considering an improvement in the disturbance rejection property by the Extended State Observer (ESO). Additionally, the ADRC is composed by a set of control features as a smooth reference obtained by the Transient Profile Generator (TRS), and a convergence technique based on a nonlinear function, which can be applied to the observer and controller gains.

This chapter presents some features about the ADRC strategy and is organized as follows: Section 3.1 discusses the motivation and the original structure of ADRC; Section 3.2 describes the formulation to obtain the smooth reference system; Section 3.3 shows the formulation of ESO; Section 3.4 describes the nonlinear weight sum and the dynamical cancellation that compose the ADRC control law; and finally, Section 3.5 shows how to compute the ADRC gains to ensure the local stability of closed-loop system.

3.1 The Original ADRC Strategy

According to Gao (2015) the ADRC strategy could be associated with a Chinese notion based on the ancestral machine called "south-pointing chariot" shown in Figure 3.1. This Chinese idea is based on the concept of ensuring the desired behavior to a linear system through the accurate measurement of internal and external disturbances, and the application of a control law that allows respectively dynamical cancellation. In the same

way, the ancestral machine "south-pointing chariot" has a gear system that measures the change of chariot's orientation and counteracts in the pointer's orientation. Therefore, in the south-pointing chariot the pointer always indicates the south orientation regardless of changing in chariot's orientation and the visibly of the environment.

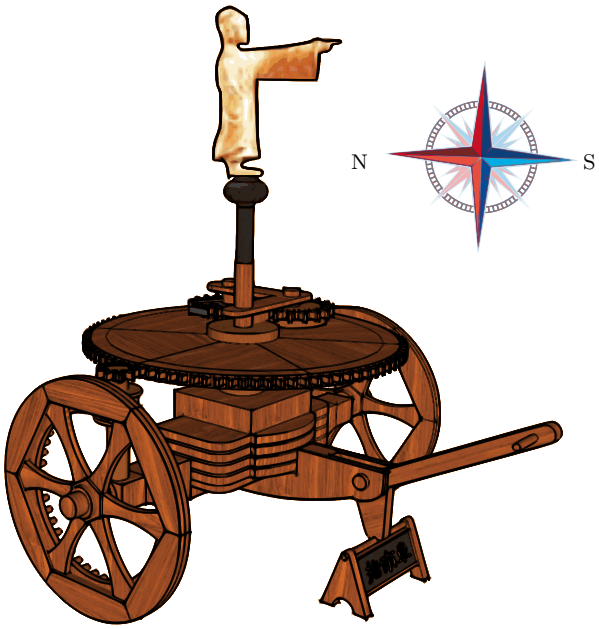

Figure 3.1: South-Pointing Chariot.

However, the original version of ADRC became known in the control area with the paper *"From PID to active disturbance rejection control"* by professor Han (2009). Its motivation was focused in developing a control strategy with the same applicability of PID controllers, but with improvements respect to the computational errors, the calculation of the time derivative, the performance of the controller due to linear gains, and the windup effect caused by the integral action. The ADRC strategy improved the computation by the transient profile generator, the noise tolerance in the tracking differentiator, the control law performance by the nonlinear gains and the disturbances rejection by the dynamical cancellation of the ADRC.

A representation of the ADRC topology is shown in Figure 3.2, where the controlled system and the main components of the ADRC strategy are illustrated: the transient profile generator, the nonlinear sum weight, and the extended state observer. It is worth noting that the plant used for the formulation of the original ADRC is defined as Single-Input Single-Output (SISO) input affine nonlinear dynamical system with a well-defined Full Relative Degree (FRD). The mathematical expression of the plant in the state-space

representation is given by

$$\begin{aligned} \dot{x}_1 &= x_2, \\ \dot{x}_2 &= F(t) + G(t)u, \\ y &= x_1, \end{aligned} \tag{3.1}$$

where $x \in \mathbb{R}^n$ is the state vector, $n = 2$ is the number of states, u is the system's input, y is the system's output, $G(t)$ is a bounded nonlinear function, and $F(t) \equiv F(x_1, x_2, w(t), t)$ is a bounded nonlinear function that contains terms of the state vector x, external disturbances $w(t)$ and time t.

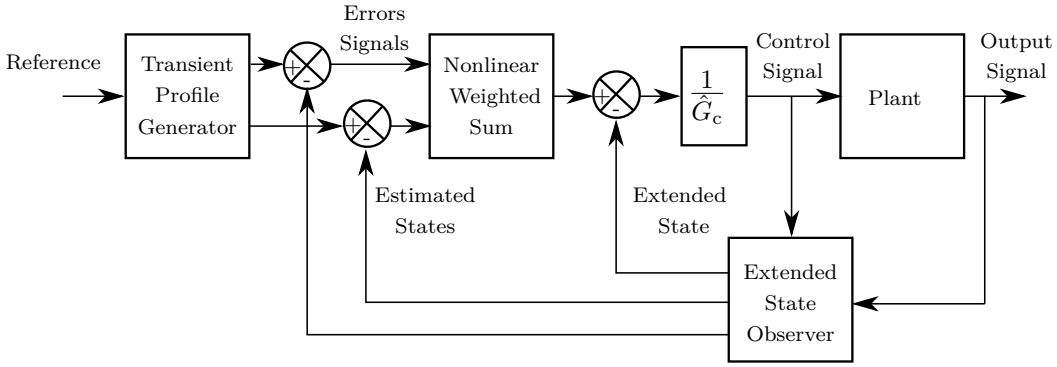

Figure 3.2: ADRC topology.

From Figure 3.2, we can see that the constant $\hat{G}_c \in \mathbb{R}$ is embedded into the control law of the ADRC structure, which is an approximated value of the nonlinear function $G(t)$ in (3.1). This constant is the only element of the ADRC strategy that does not comply with the model-free control idea. However, this constant can be obtained by trial and error tuning or by a prior knowledge of the system's model.

3.2 Transient Profile Generator

The Transient Profile Generator (TPG) is proposed in Han (2009) as a second-order dynamical system used in the ADRC to generate references, which are employed in the PD action of the ADRC control law. The main motivation to use TPG in the ADRC is to filter abrupt reference changes, which become suitable for the tracking of the system's output (Han, 2009).

The proposed TPG in Han (2009) is obtained from the time-optimal solution used to control a double integrator system (Kirk, 2012; Liberzon, 2012). The cost function employed to formulate the time-optimal control problem is given by

$$J = t_1 - t_0 = \int_{t_0}^{t_1} 1 dt,$$

where t_0 is the initial time and t_1 is the final time taken to control a double integrator system.

The time-optimal solution is obtained by using the control signal $u^* = -\operatorname{sign}(z(\zeta))$, where ζ is the state vector of the double integrator system and $z(\zeta)$ is the switch function described by

$$z(\zeta) \triangleq \zeta_1 + \frac{1}{2}\zeta_2|\zeta_2|.$$

Considering the previous control law, the TPG is formulated as

$$\begin{aligned} \dot{y}^{\mathrm{s}}_{\mathrm{ref}\,1} =& y^{\mathrm{s}}_{\mathrm{ref}\,2}, \\ \dot{y}^{\mathrm{s}}_{\mathrm{ref}\,2} =& -p_{\mathrm{s}}\operatorname{sign}\left(y^{\mathrm{s}}_{\mathrm{ref}\,1} - y_{\mathrm{ref}} + \frac{y^{\mathrm{s}}_{\mathrm{ref}\,2}|y^{\mathrm{s}}_{\mathrm{ref}\,2}|}{2p_{\mathrm{s}}}\right), \end{aligned} \tag{3.2}$$

where the TPG input y_{ref} is the reference and the TPG outputs $y^{\mathrm{s}}_{\mathrm{ref}\,1}$ and $y^{\mathrm{s}}_{\mathrm{ref}\,2}$ are the new smooth reference and its time-derivative, respectively. The constant p_{s} is the smoothing parameter, which can be chosen considering the physical limitation of the system's actuator and also according to the desired speed and smoothness of the new reference.

3.3 Extended State Observer

The state observers are necessary in control low design, when the controller does not have access of all states of the system. In the same way, in the ADRC design a state observer is required with an extended state, which estimates the external disturbances and nonlinearities of the system. This observer is called the *extended state observer*, which was proposed by Han (2009). The ESO was formulated as a third-order estimator for second-order nonlinear systems as shown in (3.1).

The key of the ESO formulation is to assume that the system (3.1) with a differentiable nonlinear function $F(t)$ can be represented by an augmented system described by

$$\begin{aligned} \dot{x}_1 &= x_2, \\ \dot{x}_2 &= x_3 + G(t)u_{\mathrm{adrc}}, \\ \dot{x}_3 &= D(t), \\ y &= x_1, \end{aligned} \tag{3.3}$$

where the system's input u_{adrc} is the control signal generated by the ADRC strategy, the extended state is $x_3 = F(t)$ and its time-derivative is $D(t) \equiv \frac{dF(t)}{dt}$.

The ESO is formulated using the extended system (3.3) and designing a Luenberger-like

observer, which is given by

$$\begin{cases} \dot{\hat{x}}_1 &= \hat{x}_2 + \ell_1(x_1 - \hat{x}_1), \\ \dot{\hat{x}}_2 &= \hat{x}_3 + \ell_2(x_1 - \hat{x}_1) + \hat{G}_c u_{\text{adrc}}, \\ \dot{\hat{x}}_3 &= \ell_3(x_1 - \hat{x}_1), \end{cases} \tag{3.4}$$

where $\hat{x}_i$ with $i = 1, 2, 3$, are the estimated states, $\hat{G}_c$ is a constant value computed as mentioned in Section 3.1, and $\ell_i(.)$, $i = 1, 2, 3$, are functions that represent the observer gains, not necessarily linear.

In this work the ESO is used with nonlinear observer gains denoted by $\ell_1 = L_1$, $\ell_2 = L_2 f_1(\tilde{x}_1, \beta_1, \varrho)$ and $\ell_3 = L_3 f_2(\tilde{x}_1, \beta_2, \varrho)$, where L_i with $i = 1, 2, 3$ are constant values and the nonlinear functions $f_i(\tilde{x}_1, \beta_i, \varrho)$ with $i = 1, 2$, are given by

$$f_i(\tilde{x}_1, \beta_i, \varrho) = \begin{cases} \frac{\tilde{x}_1}{\varrho^{1-\beta_i}}, & |\tilde{x}_1| \leq \varrho; \\ |\tilde{x}_1|^{\beta_i} \text{sign}(\tilde{x}_1), & |\tilde{x}_1| > \varrho, \end{cases} \tag{3.5}$$

where $\tilde{x}_1 \equiv x_1 - \hat{x}_1$ is the observer error, ϱ is a scalar that represents the error limit of change in the convergence velocity, and β_i is a scalar that represents the rate of convergence velocity, which is chosen such that $\beta_i < \varrho$ and $\beta_i < 1$.

The objective of applying the convergence technique represented by the nonlinear functions $f_i(\tilde{x}_1, \beta_i, \varrho)$ is to improve the convergence time, such that when the observer has a large error then its gains are small. On the opposite case, its gains are large, consequently, a smooth convergence of observer is obtained . Clearly, the structure in (3.4) can be seen as a Unknown Input Observer (UIO) (Takahashi & Peres, 1999) with $D(t)$ and $(G(t) - \hat{G}_c)u(t)$ as unknown inputs, such that the observer state $\hat{x}_3$ is used as an estimative for $F(t)$ in (3.1), i.e. $\hat{F}(t) = \hat{x}_3$ in (3.3).

Finally, the ESO, including the nonlinear function, is given by

$$\begin{cases} \dot{\hat{x}}_1 &= \hat{x}_2 + L_1(\tilde{x}_1), \\ \dot{\hat{x}}_2 &= \hat{x}_3 + L_2 f_1(\tilde{x}_1, \beta_1, \varrho) + \hat{G}_c u_{\text{adrc}}, \\ \dot{\hat{x}}_3 &= L_3 f_2(\tilde{x}_1, \beta_2, \varrho), \end{cases} \tag{3.6}$$

It is important to mention that the ESO representation, when the function $F(t)$ of the nonlinear system (3.1) contains some dependence on x_2, must have the input $\hat{G}_c u_{\text{adrc}}$ in the equation of $\dot{\hat{x}}_3$. However, if the terms of $F(t)$ are known, the ADRC strategy would lose its "model-free" property.

On the other hand, it is worth noting that all estimated states by the ESO depend on the measured variable x_1. Hence, the performance of ESO is affected by the quality of the output signal obtained from the system.

3.4 Nonlinear Weighted Sum and Dynamical Cancellation

The ADRC control law is designed with two complementary actions: i) a PD control based on a nonlinear weighted sum; and ii) a dynamical cancellation based on the disturbance estimation obtained by the ESO. Thereby, the ADRC strategy has a similar control law to the feedback linearization control, which presents a dynamical cancellation given by $\hat{F}(t)$. Contrary to the feedback linearization controller, the ADRC strategy does not use information from the mathematical model. It only uses the estimated information provided by ESO and requires the tuning of the parameter $\hat{G}_C$ in its control law. For this reason, the ADRC is considered as a "model-free" control technique and its control law is given by

$$u_{\text{adrc}} = \frac{1}{\hat{G}_{\text{c}}} \left(-\hat{F}(t) + u_{\text{vc}} \right), \tag{3.7}$$

where $\hat{G}_c$ is a constant value computed as mentioned in Section 3.1, $\hat{F}(t)$ is the extended state estimated by ESO, and the virtual control u_{vc} is a function of the tracking error and its time-derivative, i.e., a Proportional and Derivative (PD) controller. The virtual control is obtained as

$$u_{\text{vc}} = K_{\text{p}} e_{\text{a1}} + K_{\text{d}} e_{\text{a2}}, \tag{3.8}$$

where $e_{\text{a1}} = y^{\text{s}}_{\text{ref}} - \hat{x}_1$ and $e_{\text{a2}} = \dot{y}^{\text{s}}_{\text{ref}} - \hat{x}_2$ are the errors computed by ADRC, and K_{p} and K_{d} are scalars, known as controller gains. In the same way of the observer gains, they are not necessarily linear and can be defined using the nonlinear function (3.5). However, in this work linear gains are used.

Note that the TRS model defined in Section 2.4 is a third-order system and the original ADRC strategy shown in this chapter is designed to control a second-order system. Therefore, the original ADRC has presented some limitations of controlling the TRS.

3.5 ADRC Stability Analysis

This section deals with the stability proof of the ADRC. We can proof the stability of a nonlinear system in closed-loop with ADRC and, in the same way, we can compute the observer and controller gains. The stability proof of the ADRC strategy is an interesting issue, which was not full addressed by professor Han. However, some researchers in the control area have developed stability proofs for linear systems in closed-loop with ADRC (Gao, 2006), bounded nonlinear dynamics systems in closed-loop with ADRC (Zheng, 2009), and the local asymptotic stability proof for nonlinear systems in closed-loop with ADRC (Li et al., 2016).

In this work, we present the stability proof developed by Zheng (2009), which considers

two types of ESO models for nonlinear system with order n. The first ESO model assumes that the nonlinear function $D(t)$ in the extended representation (3.3) is known; the second ESO model has the similar structure of the original ADRC proposed by professor Han, where the nonlinear function $D(t)$ is unknown but bounded.

The stability analysis for nonlinear systems developed by Zheng is presented in two sections: Section 3.5.1 presents the ESO convergence analysis, and Section 3.5.2 presents the ADRC control law convergence.

3.5.1 ESO Convergence

As commented before, the systems for which the ADRC strategy is applied are defined as SISO input affine nonlinear dynamical system of the second-order and with a well-defined FRD shown in (3.1).

A first assumption is regarded that the nonlinear system (3.1) can be represented by the extended representation shown in (3.3). However, it is worth noting that when the extended representation is used, we assume that the extended state's initial conditions represent the same state's initial condition of the original nonlinear system (3.1). Otherwise, the initial responses of the extended and the original systems would be different.

The ESO (3.4) defined in Section 3.3 is used to carry out the stability proof. Nevertheless, the observer gains $\ell_i(.)$, with $i = 1, 2, 3$, are defined with respect to the observer bandwidth w_{o} and the parameter $\alpha_{\text{o}i}$, with $i = 1, 2, 3$. Hence, the gain vector is expressed by $[\ell_1, \ell_2, \ell_3] = [w_{\text{o}}\alpha_{\text{o}1}, w_{\text{o}}^2\alpha_{\text{o}2}, w_{\text{o}}^3\alpha_{\text{o}3}]$. Thereby, the ESO formulated with the observer bandwidth is given by

$$\begin{cases} \dot{\hat{x}}_1 &= \hat{x}_2 + w_{\text{o}}\alpha_{\text{o}1}(x_1 - \hat{x}_1), \\ \dot{\hat{x}}_2 &= \hat{x}_3 + w_{\text{o}}^2\alpha_{\text{o}2}(x_1 - \hat{x}_1) + \hat{G}_{\text{c}}u_{\text{adrc}}, \\ \dot{\hat{x}}_3 &= w_{\text{o}}^3\alpha_{\text{o}3}(x_1 - \hat{x}_1), \end{cases}$$

where the parameters $\alpha_{\text{o}i}$, with $i = 1, 2, 3$, are chosen such as the characteristic polynomial $s^3 + \alpha_{\text{o}1}s^2 + \alpha_{\text{o}2}s + \alpha_{\text{o}3}$ is Hurwitz. We have used the characteristic polynomial as $s^3 + w_{\text{o}}\alpha_{\text{o}1}s^2 + w_{\text{o}}^2\alpha_{\text{o}2}s + w_{\text{o}}^3\alpha_{\text{o}3} = (s + w_{\text{o}})^3$, with $\alpha_i = \frac{3!}{i!(3-i)!}$ for $i = 1, 2, 3$.

In order to prove the ESO convergence, the observer error is defined as $\tilde{x} = x - \hat{x}$ and it is assumed that the difference between G and $\hat{G}$ can be considered as disturbance, hence $\hat{G}_{\text{c}} \equiv G$. Consequently, the observer error dynamics are described by

$$\begin{cases} \dot{\tilde{x}}_1 &= \tilde{x}_2 - w_{\text{o}}\alpha_{\text{o}1}(x_1 - \hat{x}_1), \\ \dot{\tilde{x}}_2 &= \tilde{x}_3 - w_{\text{o}}^2\alpha_{\text{o}2}(x_1 - \hat{x}_1), \\ \dot{\tilde{x}}_3 &= D(t) - w_{\text{o}}^3\alpha_{\text{o}3}(x_1 - \hat{x}_1). \end{cases} \tag{3.9}$$

Using the variable transformation $\xi_i = \frac{\tilde{x}_i}{{w_{\text{o}}}^{i-1}}$, with $i = 1, 2, 3$, we can rewrite the observer

error dynamics (3.9) in a matrix form as follows

$$\dot{\xi} = w_{\text{o}} A_{\text{o}} \xi + B_{\text{o}} \frac{D(t)}{w_{\text{o}}^2}, \tag{3.10}$$

where the matrices $A_{\text{o}} \in \mathbb{R}^{3\times3}$ and $B_0 \in \mathbb{R}^{3\times1}$ are shown in (3.11) and (3.12), respectively.

$$A_{\text{o}} = \begin{bmatrix} -\alpha_{\text{o}1} & 1 & 0 \\ -\alpha_{\text{o}2} & 0 & 1 \\ -\alpha_{\text{o}3} & 0 & 0 \end{bmatrix}. \tag{3.11}$$

$$B_{\text{o}} = \begin{bmatrix} 0 & 0 & 1 \end{bmatrix}^T. \tag{3.12}$$

Theorem 1. *(Zheng, 2009, Theorem 2)*

Assuming $D(t)$ is bounded, there exist constants $\sigma_i > 0$ and a finite $T_1 > 0$ such that $|\tilde{x}_i| \leq \sigma_i$ where $\tilde{x}_i = x_i - \hat{x}_i$ with $i = 1, 2, 3$, $\forall t \geq T_1 > 0$ and $w_o > 0$. Furthermore, $\sigma_i = O(\frac{1}{w_o^k})$, for some positive integer k, where O is the big O notation[1].

Proof. Solving the differential equation (3.10), we obtain

$$\xi(t) = e^{w_{\text{o}} A_{\text{o}} t}\xi(0) + \int_0^t e^{w_{\text{o}} A_{\text{o}}(t-\tau)} B \frac{D(t)}{w_{\text{o}}^2} d\tau, \tag{3.13}$$

where $D(t)$ is the time-derivative of $F(t)$. We take a part to solve, which is described by

$$p(t) = \int_0^t e^{w_{\text{o}} A_{\text{o}}(t-\tau)} B \frac{D(t)}{w_{\text{o}}^2} d\tau. \tag{3.14}$$

Since $D(t)$ is bounded, we can define that $|D(t)| \leq \delta$, where δ is a positive constant. Considering the states x_i with $i = 1, 2, 3$ and δ, the equation (3.14) can be described as

$$\begin{aligned} |p_i| \leq & \frac{\int_0^t [e^{w_{\text{o}} A_{\text{o}}(t-\tau)} B_{\text{o}}]_i |D(x(\tau), w(t), t)| d\tau}{w_o^2}; \\ \leq & \frac{\delta \int_0^t [e^{w_{\text{o}} A_{\text{o}}(t-\tau)} B_{\text{o}}]_i d\tau}{w_o^2}; \\ = & \frac{\delta}{w_o^2} \left\{ \left[-(w_{\text{o}} A_{\text{o}})^{-1} e^{w_{\text{o}} A_{\text{o}}(t-\tau)} |_0^t \right] B_{\text{o}} \right\}_i; \\ \leq & \frac{\delta}{w_{\text{o}}^3} [|(A_{\text{o}}^{-1} B_{\text{o}})_i| + |(A_{\text{o}}^{-1} e^{w_{\text{o}} A_{\text{o}} t} B_{\text{o}})_i|]. \end{aligned} \tag{3.15}$$

Using A_{o} and B_{o} defined in (3.11) and (3.12), respectively. We have that A_{o}^{-1} is given by

$$A_{\text{o}}^{-1} = \begin{bmatrix} 0 & 0 & -\frac{1}{\alpha_{\text{o}3}} \\ 1 & 0 & -\frac{\alpha_{\text{o}1}}{\alpha_{\text{o}3}} \\ 0 & 1 & -\frac{\alpha_{\text{o}2}}{\alpha_{\text{o}3}} \end{bmatrix},$$

[1]The big O notation denotes the limiting behavior of a function when the argument tends towards a particular value or infinite.

and $|(A_{\mathrm{o}}^{-1}B_{\mathrm{o}})_i|$ is given by

$$\begin{aligned}|(A_{\mathrm{o}}^{-1}B_{\mathrm{o}})_i| =& \left|\begin{bmatrix} -\frac{1}{\alpha_{\mathrm{o}3}} \\ -\frac{\alpha_{\mathrm{o}1}}{\alpha_{\mathrm{o}3}} \\ -\frac{\alpha_{\mathrm{o}2}}{\alpha_{\mathrm{o}3}} \end{bmatrix}_i\right|; \\ =& \begin{cases} \frac{1}{\alpha_{\mathrm{o}3}}\Big|_{i=1} \\ \frac{\alpha_{\mathrm{o}i-1}}{\alpha_{\mathrm{o}3}}\Big|_{i=2,3} \end{cases}; \\ \leq& v,\end{aligned} \tag{3.16}$$

where it is assumed that $v = \max_{i=1,2,3}\left\{\frac{1}{\alpha_{\mathrm{o}3}}, \frac{\alpha_{\mathrm{o}i-1}}{\alpha_{\mathrm{o}3}}\right\}$. With A_{o} Hurwitz there exists a finite time $T_1 > 0$ for all $t \geq T_1$ with $i, j = 1, 2, 3$ such that satisfies

$$|[e^{w_{\mathrm{o}}A_{\mathrm{o}}t}]_{ij}| \leq \frac{1}{w_{\mathrm{o}}^3}.$$

Therefore, for all $t \geq T_1$ with $i = 1, 2, 3$, we have

$$|[e^{w_{\mathrm{o}}A_{\mathrm{o}}t}B_{\mathrm{o}}]_i| \leq \frac{1}{w_{\mathrm{o}}^3}.$$

Note that T_1 depends on $w_{\mathrm{o}}A_{\mathrm{o}}$. The matrices A_{o} and $e^{w_{\mathrm{o}}A_{\mathrm{o}}t}$ can be rewritten as shown in

$$A_{\mathrm{o}}^{-1} = \begin{bmatrix} b_{11} & b_{12} & b_{13} \\ b_{21} & b_{22} & b_{23} \\ b_{31} & b_{32} & b_{33} \end{bmatrix}, \tag{3.17}$$

$$e^{w_{\mathrm{o}}A_{\mathrm{o}}t} = \begin{bmatrix} d_{11} & d_{12} & d_{13} \\ d_{21} & d_{22} & d_{23} \\ d_{31} & d_{32} & d_{33} \end{bmatrix}. \tag{3.18}$$

Using (3.17) and (3.18), we have that $|(A_{\mathrm{o}}^{-1}e^{w_{\mathrm{o}}A_{\mathrm{o}}t}B_{\mathrm{o}})_i|$ is described by

$$\begin{aligned}|(A_{\mathrm{o}}^{-1}e^{w_{\mathrm{o}}A_{\mathrm{o}}t}B_{\mathrm{o}})_i| =& |b_{i1}d_{13} + b_{i2}d_{23} + b_{i3}d_{33}|; \\ \leq& \frac{|b_{i1}| + |b_{i2}| + |b_{i3}|}{w_{\mathrm{o}}^3}; \\ =& \begin{cases} \frac{1}{w_{\mathrm{o}}^3\alpha_{\mathrm{o}3}}\Big|_{i=1}; \\ \frac{1}{w_{\mathrm{o}}^3}(1 + \frac{\alpha_{\mathrm{o}i-1}}{\alpha_{\mathrm{o}3}})\Big|_{i=2,3}; \end{cases} \\ \leq& \frac{\eta}{w_{\mathrm{o}}^3},\end{aligned} \tag{3.19}$$

where it is assumed that $\eta = \max_{i=1,2,3}\left\{\frac{1}{\alpha_{\mathrm{o}3}}, 1 + \frac{\alpha_{\mathrm{o}i-1}}{\alpha_{\mathrm{o}3}}\right\}$ for all $t \geq T_1$ with $i = 1, 2, 3$.

Substituting (3.16) and (3.19) in (3.15), we can rewrite $|p_i(t)|$ as shown in

$$|p_i(t)| \leq \frac{\delta v}{w_{\mathrm{o}}^3} + \frac{\delta \eta}{w_{\mathrm{o}}^6},$$

for all $t \geq T_1$ with $i = 1, 2, 3$. The expression $|[e^{w_{\mathrm{o}} A_{\mathrm{o}} t} \xi(0)]_i|$ from (3.13) is given by

$$\begin{aligned} |[e^{w_{\mathrm{o}} A_{\mathrm{o}} t} \xi(0)]_i| =& |d_{i1}\xi_1(0) + d_{i2}\xi_2(0) + d_{i3}\xi_3(0)|; \\ \leq& \frac{\xi_{sum}(0)}{w_{\mathrm{o}}^3}, \end{aligned}$$

where $\xi_{sum}(0) = |\xi_1(0)| + |\xi_2(0)| + |\xi_3(0)|$ is considered for all $t = T_1$ with $i = 1, 2, 3$.

The equation (3.13) can be rewritten as

$$|\xi_i(t)| \leq |[e^{w_{\mathrm{o}} A_{\mathrm{o}} t} \xi(0)]_i| + |p_i(t)|. \tag{3.20}$$

Finally, a variable transformation is applied defined by $\xi_i = \frac{\tilde{x}_i}{w_{\mathrm{o}}^{i-1}}$ in (3.20), giving

$$\begin{aligned} |\tilde{x}_i(t)| &\leq \left| \frac{\xi_{sum}(0)}{w_{\mathrm{o}}^3} \right| w_{\mathrm{o}}^{i-1} + |p_i(t)| w_{\mathrm{o}}^{i-1}; \\ &\leq \left| \frac{\tilde{x}_{sum}(0)}{w_{\mathrm{o}}^3} \right| + \frac{\delta v}{w_{\mathrm{o}}^{4-i}} + \frac{\delta \eta}{w_{\mathrm{o}}^{7-i}}; \\ &= \sigma_i, \end{aligned} \tag{3.21}$$

where $\tilde{x}_{sum}(0) = |\tilde{x}_1(0)| + |\tilde{x}_2(0)| + |\tilde{x}_3(0)|$ for all $t \geq T_i$ with $i = 1, 2, 3$ is assumed.

Hence, it is demonstrated that $|\tilde{x}_i(t)| = \sigma_i$ for all $t \geq T_1$ with $i = 1, 2, 3$. Q.E.D.

□

It is important to highlight that for the fulfillment of the Theorem 1, the nonlinear function $D(t)$ must be bounded and it is assumed that parameter $\hat{G}_{\mathrm{c}} \equiv G$. In this case, the Theorem 1 shows that the error dynamics of ESO is bounded and there exists an upper bound that monotonously decreases with the observer bandwidth w_{o}.

3.5.2 ADRC Control Law Convergence

The ADRC control law proposed by Han (2009) was modified in the stability proof proposed by Zheng (2009), in which the ADRC control law includes an additional time-derivative of the reference, being formulated for nonlinear systems of n order.

In this work, we show the stability proof of the ADRC convergence developed by Zheng (2009), which uses the ADRC control law given by

$$u_{\mathrm{adrc}}^* = \frac{1}{\hat{G}_{\mathrm{c}}}(-\hat{x}_3 + \ddot{y}_{\mathrm{ref}}^{\mathrm{s}} + K_{\mathrm{p}} e_{\mathrm{a1}} + K_{\mathrm{d}} e_{\mathrm{a2}}),$$

where $\ddot{y}^{\mathrm{s}}_{\mathrm{ref}}$ is the second time-derivative of the smooth reference.

Assuming that the nonlinear system (3.1) can be represented by the extended system (3.3), and the parameter $\hat{G}_{\mathrm{c}} \equiv G$, then we have the nonlinear system in closed-loop given by

$$\begin{aligned} \dot{x}_1 &= x_2, \\ \dot{x}_2 &= x_3 - \hat{x}_3 + \ddot{y}^{\mathrm{s}}_{\mathrm{ref}} + K_{\mathrm{p}} e_{\mathrm{a1}} + K_{\mathrm{d}} e_{\mathrm{a2}}, \\ \dot{x}_3 &= D(t). \end{aligned} \tag{3.22}$$

Substituting the error $e_{\mathrm{a1}} = y^{\mathrm{s}}_{\mathrm{ref}} - \hat{x}_1$ and $e_{\mathrm{a2}} = \dot{y}^{\mathrm{s}}_{\mathrm{ref}} - \hat{x}_1$ in the closed-loop system (3.22), and considering the observer error $\tilde{x}_i = x_i - \hat{x}_i$ with $i = 1, 2$, the following closed-loop system is obtained

$$\begin{aligned} \dot{x}_1 &= x_2, \\ \dot{x}_2 &= x_3 - \hat{x}_3 + \ddot{y}^{\mathrm{s}}_{\mathrm{ref}} + K_{\mathrm{p}}(y^{\mathrm{s}}_{\mathrm{ref}} - x_1 + \tilde{x}_1) + K_{\mathrm{d}}(\dot{y}^{\mathrm{s}}_{\mathrm{ref}} - x_2 + \tilde{x}_2), \\ \dot{x}_3 &= D(t). \end{aligned} \tag{3.23}$$

With the controller error defined by $e_{\mathrm{c}i} = \frac{d^{i-1}}{dt^{i-1}}(y^{\mathrm{s}}_{\mathrm{ref}}) - x_i$ with $i = 1, 2$, its dynamics are given by

$$\begin{aligned} \dot{e}_{\mathrm{c1}} &= \dot{y}^{\mathrm{s}}_{\mathrm{ref}} - \dot{x}_1, \\ \dot{e}_{\mathrm{c2}} &= \ddot{y}^{\mathrm{s}}_{\mathrm{ref}} - \dot{x}_2. \end{aligned} \tag{3.24}$$

Substituting the closed-loop system (3.23) in the controller error dynamics (3.24) yields

$$\begin{aligned} \dot{e}_{\mathrm{c1}} &= \dot{y}^{\mathrm{s}}_{\mathrm{ref}} - x_2; \\ &= e_{\mathrm{c2}}, \\ \dot{e}_{\mathrm{c2}} &= \ddot{y}^{\mathrm{s}}_{\mathrm{ref}} - (x_3 - \hat{x}_3 + \ddot{y}^{\mathrm{s}}_{\mathrm{ref}} + K_{\mathrm{p}}(y^{\mathrm{s}}_{\mathrm{ref}} - x_1 + \tilde{x}_1) + K_{\mathrm{d}}(\dot{y}^{\mathrm{s}}_{\mathrm{ref}} - x_2 + \tilde{x}_2)); \\ &= -x_3 + \hat{x}_3 - K_{\mathrm{p}}(e_{\mathrm{c1}} + \tilde{x}_1) - K_{\mathrm{d}}(e_{\mathrm{c2}} + \tilde{x}_2). \end{aligned}$$

Using the observer error $\tilde{x} = x - \hat{x}$ for x_3, the equations of the controller error dynamics are given by

$$\begin{aligned} \dot{e}_{\mathrm{c1}} &= e_{\mathrm{c2}}, \\ \dot{e}_{\mathrm{c2}} &= -K_{\mathrm{p}} e_{\mathrm{c1}} - K_{\mathrm{d}} e_{\mathrm{c2}} - K_{\mathrm{p}} \tilde{x}_1 - K_{\mathrm{d}} \tilde{x}_2 - \tilde{x}_3. \end{aligned} \tag{3.25}$$

Let $e_{\mathrm{c}} = [e_{\mathrm{c1}} e_{\mathrm{c2}}]^T$ and $\tilde{x} = [\tilde{x}_1 \tilde{x}_2 \tilde{x}_3]^T$, the controller error dynamics can be represented (3.25) in matrix form by

$$\dot{e}_{\mathrm{c}} = A_{\mathrm{ec}} e_{\mathrm{c}} + A_{\tilde{x}} \tilde{x}, \tag{3.26}$$

where $A_{\mathrm{ec}} \in \mathbb{R}^{2\times 2}$ and $A_{\tilde{x}} \in \mathbb{R}^{2\times 2}$ are given by

$$A_{\mathrm{ec}} = \begin{bmatrix} 0 & 1 \\ -K_{\mathrm{p}} & -K_{\mathrm{d}} \end{bmatrix}, \tag{3.27}$$

$$A_{\tilde{x}} = \begin{bmatrix} 0 & 0 & 0 \\ -K_p & -K_{\mathrm{d}} & -1 \end{bmatrix}. \tag{3.28}$$

Theorem 2. *(Zheng, 2009, Theorem 4) Assuming D(t) is bounded, there exist constants* $\rho_i > 0$ *and a finite* $T_3 > 0$ *such that* $|e_{ci}| \leq \rho_i$ *where* $e_{ci} = \frac{d^{i-1}}{dt^{i-1}}(y^s_{ref}) - x_i$ *with* $i = 1, 2, 3$, $\forall t \geq T_3 > 0$, $w_o > 0$, *and* $w_c > 0$. *Furthermore,* $\rho_i = O(\frac{1}{w_c^r})$, *for some positive integer* r.

Proof. Solving the differential equation (3.26), we obtain

$$e_{\mathrm{c}}(t) = e^{A_{\mathrm{ec}}t}e_{\mathrm{c}}(0) + \int_0^t e^{A_{\mathrm{ec}}(t-\tau)}A_{\tilde{x}}\tilde{x}(\tau)d\tau. \tag{3.29}$$

With (3.26) and according to the Theorem 1, for all $t \geq T_1$, it is obtained

$$\begin{aligned} [A_{\tilde{x}}\tilde{x}(\tau)]_{i=1,2} &= 0, \\ |[A_{\tilde{x}}\tilde{x}(\tau)]_3| &= |-K_{\mathrm{p}}\tilde{x}_1(\tau) - K_{\mathrm{d}}\tilde{x}_3(\tau) - \tilde{x}_3(\tau)|; \\ &\leq K_{sum}\sigma_i = \gamma, \end{aligned} \tag{3.30}$$

where $K_{sum} = 1 + K_{\mathrm{p}} + K_{\mathrm{d}}$. The parameters K_{p} and K_{d} are scalars, which are chosen such that the characteristic polynomial $s^2 + K_{\mathrm{d}}s^1 + K_{\mathrm{p}}$ is Hurwitz. In other words, A_{ec} is chosen Hurwitz.

We used the characteristic polynomial given by $s^2 + K_{\mathrm{d}}s^1 + K_{\mathrm{p}} = (s + w_{\mathrm{c}})^2$, where the controller bandwidth $w_{\mathrm{c}} > 0$ is included. Considering the parameters $K_{\mathrm{p}} = K_1$ and $K_{\mathrm{d}} = K_2$, we can represent them by $K_i = \frac{2!}{(i-1)!(3-i)!}w_{\mathrm{c}}^{3-i}$, with $i = 1, 2$.

Defining $\Psi = [0\ \gamma]^T$, we can rewrite a part from (3.29) given by $\vartheta(t) = \int_0^t e^{A_{\mathrm{ec}}(t-\tau)}A_{\tilde{x}}\tilde{x}(\tau)d\tau$ as shown

$$\begin{aligned} |\vartheta_i(t)| &= \int_0^t [e^{A_{\mathrm{ec}}(t-\tau)}A_{\tilde{x}}\tilde{x}(\tau)]_i d\tau; \\ &\leq \int_0^t [e^{A_{\mathrm{ec}}(t-\tau)}\Psi]_i d\tau; \\ &= \left\{\left[-A_{\mathrm{ec}}^{-1}e^{A_{\mathrm{ec}}(t-\tau)}\big|_0^t\right]\Psi\right\}_i; \\ &\leq |(A_{\mathrm{ec}}^{-1}\Psi)_i| + |((A_{\mathrm{ec}}^{-1}e^{A_{\mathrm{ec}}t}\Psi)_i|. \end{aligned} \tag{3.31}$$

With A_{ec} (3.27) and Ψ, we can compute A_{ec}^{-1} and $A_{\mathrm{ec}}^{-1}\Psi$ as

$$A_{\mathrm{ec}}^{-1} = \begin{bmatrix} -\frac{K_{\mathrm{d}}}{K_{\mathrm{p}}} & -\frac{1}{K_{\mathrm{p}}} \\ 1 & 0 \end{bmatrix}, \tag{3.32}$$

$$\begin{aligned} |(A_{\mathrm{ec}}^{-1}\Psi)_1| &= \frac{\gamma}{K_{\mathrm{p}}} = \frac{\gamma}{w_c^2}, \\ |(A_{\mathrm{ec}}^{-1}\Psi)_2| &= 0. \end{aligned} \tag{3.33}$$

Since A_{ec} is Hurwitz, there exists a finite time $T_2 > 0$ for all $t \geq T_2$ with $i, j = 1, 2$ such that it satisfies

$$|[e^{A_{\mathrm{ec}}t}]_{ij}| \leq \frac{1}{w_c^3}.$$

Note that T_2 depends on A_{ec}. Let $T_3 = \max\{T_1, T_2\}$, we have $|[e^{A_{\mathrm{ec}}t}\Psi]_i|$, for all $t \geq T_3$ with $i = 1, 2$, given by

$$|[e^{A_{\mathrm{ec}}t}\Psi]_i| \leq \frac{\gamma}{w_c^3}. \tag{3.34}$$

Using (3.32) and (3.34), we can compute $|(A_{\mathrm{ec}}^{-1}e^{A_{\mathrm{ec}}t}\Psi)_i|$ for all $t \geq T_3$, which is given by

$$|(A_{\mathrm{ec}}^{-1}e^{A_{\mathrm{ec}}t}\Psi)_i| \leq \begin{cases} \frac{1+K_2}{w_{\mathrm{c}}^2}\frac{\gamma}{w_{\mathrm{c}}^3}\Big|_{i=1}; \\ \frac{\gamma}{w_{\mathrm{c}}^3}\Big|_{i=2}. \end{cases} \tag{3.35}$$

Substituting (3.33) and (3.35) in (3.31), we can rewrite $|\vartheta_i(t)|$ for all $t \geq T_3$, as

$$\begin{aligned} |\vartheta_i(t)| &\leq |(A_{\mathrm{ec}}^{-1}\Psi)_i| + |(A_{\mathrm{ec}}^{-1}e^{A_{\mathrm{ec}}t}\Psi)_i|; \\ &\leq \begin{cases} \frac{\gamma}{w_{\mathrm{c}}^2} + \frac{1+K_2}{w_{\mathrm{c}}^2}\frac{\gamma}{w_{\mathrm{c}}^3}\Big|_{i=1}; \\ \frac{\gamma}{w_{\mathrm{c}}^3}\Big|_{i=2}. \end{cases} \end{aligned} \tag{3.36}$$

We can compute $|[e^{A_{\mathrm{ec}}t}e_{\mathrm{c}}(0)]_i|$ from (3.29), considering $e^{A_{\mathrm{ec}}t} = \begin{bmatrix} O_{11} & O_{12} \\ O_{21} & O_{22} \end{bmatrix}$ and $e_{csum}(0) = |e_{\mathrm{c}1}(0)| + |e_{\mathrm{c}2}(0)|$ for all $t = T_3$ with $i = 1, 2$, which is described by

$$\begin{aligned} |[e^{A_{\mathrm{ec}}t}e_{\mathrm{c}}(0)]_i| &= |O_{i1}e_{\mathrm{c}1}(0) + O_{i2}e_{\mathrm{c}2}(0)|; \\ &\leq \frac{e_{csum}(0)}{w_{\mathrm{c}}^3}. \end{aligned} \tag{3.37}$$

Using (3.31), we can rewrite the solution of differential equation (3.29) as shown

$$|e_{ci}(t)| \leq |[e^{A_{\mathrm{ec}}t}e_{\mathrm{c}}(0)]_i| + |\vartheta_i(t)|. \tag{3.38}$$

Finally, using (3.30), and substituting (3.36) and (3.37) in equation (3.38), we can compute

$|e_{ci}(t)|$ for all $t \geq T_3$ with $i = 1, 2$, which is given by

$$|e_{ci}(t)| \leq \begin{cases} \frac{e_{csum}(0)}{w_c^3} + \frac{K_{sum}\sigma_i}{w_c^2} + \frac{(1+K_2)K_{sum}\sigma_i}{w_c^5}\Big|_{i=1}; \\ \frac{e_{csum}(0)+K_{sum}\sigma_i}{w_c^3}\Big|_{i=2}; \end{cases}$$
$$\leq \rho_i,$$

where $\rho = \max\left\{\frac{e_{csum}(0)}{w_c^3} + \frac{K_{sum}\sigma}{w_c^2} + \frac{(1+K_2)K_{sum}\sigma}{w_c^5}, \frac{e_{csum}(0)+K_{sum}\sigma}{w_c^3}\right\}$.

Hence, it is demonstrated that $|e_{ci}(t)| \leq \rho_i$ for all $t \geq T_3$ with $i = 1, 2$. Q.E.D.

□

In the same way of Theorem 1, it is worthwhile to note that for the fulfillment of the Theorem 2, the nonlinear function $D(t)$ must be bounded, the parameter $\hat{G}_c \equiv G$, and the virtual control u_{cv} proposed by professor Han (2009) is modified with the inclusion of the second time-derivative of reference. In this case, the Theorem 2 shows that in the nonlinear system (3.1) in closed-loop with ADRC, the tracking error is bounded and its upper bounds monotonously decrease with the observer w_o and controller w_c bandwidths.

3.6 Final Remarks

This chapter presented the main motivations of the original ADRC and its main components, which were proposed by Han (2009). It was defined the set of the nonlinear systems in which the ADRC strategy can be applied.

The ADRC formulation and the functionality of its components, such as the transient profile generator, the extended state observer, and the ADRC control law, were explained with their assumptions. This ADRC scheme is used in the Chapters 4 and 5.

The stability proof of the ESO and the ADRC convergence proposed by Zheng (2009) were presented. This stability analysis considered that the controlled nonlinear dynamics of the system is bounded, and in the ADRC control is included the second time-derivative of the reference.

4

A Modified ADRC Strategy

In the previous chapter each of the elements that make up the original ADRC strategy proposed by professor Han were defined. However, with the objective of using the ADRC for controlling the TRS, we propose a modification in the original ADRC structure by adding two elements to improve the performance of the closed-loop system. Particular characteristics of the TRS are considered as presented in Chapter 2, mainly the measurement output quantization effect.

This chapter is organized follows: Section 4.1 introduces the main motivations for the proposed ADRC modifications; Section 4.2 describes two differentiation methods useful in the modified ADRC; Section 4.3 presents the modified ADRC strategy; Section 4.4 shows simulation results of the TRS in closed-loop; and finally, Section 4.5 presents the concluding remarks.

4.1 Motivations

As commented before, the quantization error caused by the incremental encoder in a system's output is a common issue in signal processing and control areas. For example, this problem can affects the feedback control strategies that rely on an observer for state estimation. In this case the abrupt changes in the measured output, caused by quantization effects, result in the injection of high frequency noise in the observer. This issue is challenging, mainly when the observer is employed to provide estimates of time-derivative of the output signal, since it is well-known that differentiation tends to amplify

the noise (Mboup et al., 2009).

A well-known solution to improve the state estimation when the system's output presents quantization is to implement a low-pass filter in the observer's input. This alternative introduces an unavoidable time-delay. Furthermore, the dynamics of the low-pass filter require a convergence analysis as it is discussed in Olfati-Saber & Shamma (2005).

In this work we propose to use a smooth approximation of the system's output by means of a polynomial time function obtained through an Algebraic Differentiation Procedure (ADP), as presented in Section 4.2.1. As a low-pass filter, this smooth approximation introduces time-delay, but the ADP can be implemented as a linear Finite Impulse Response (FIR) digital filter and, thereby, it is always stable.

In addition, it is important to note that the TRS is represented by a third order nonlinear system (Chapter 2), and the original ADRC was formulated for second order nonlinear systems. Therefore, with the goal of using the original ADRC structure, we provisionally consider that the TRS dynamics is directly excited by the propulsion torque T_{p}. Since T_{p} actually depends on the third state variable x_3; namely the main rotor angular speed, ω, in (2.5) (on page 13); we use a dynamical cancellation – or Inverse Dynamics (ID) – strategy, that depends on the estimation of this state variable, to have an approximated second-order system. The estimation procedure is based on the computation of the time-derivative of the output, which is obtained by using a Robust and Exact Differentiator (RED) briefly discussed in Section 4.2.2. It is worthwhile to mention that the mathematical expression is only an approximated dynamical cancellation, and it is not robust to parametric uncertainties. Indeed, in this chapter we analyze the results obtained in TRS' simulations in closed-loop using the ADRC strategy with and without ID.

4.2 Differentiation Methods

In this section we describe the mathematical formulation, advantages and disadvantages, applications, and the role played in the differences in performance between the two differentiator techniques (ADP and RED) when used in the modified ADRC.

4.2.1 Algebraic Differentiation Procedure (ADP)

The ADP is the product of the research initiated by Fliess & Sira-Ramírez (2003), who continued working with the same algebraic framework for various control questions as shown in Fliess & Sira-Ramírez (2004). In this work a preliminary version of the algebraic derivative estimation method was first presented, followed by Reger et al. (2005), where the ADP employed can be found. A few years later Mboup et al. (2009) published a comprehensive paper on the numerical differentiation with annihilators in a noisy

environment based on the algebraic approach.

The ADP formulation is derived by the mathematical manipulation of the Taylor-series expansion of a signal in time, using the rules of the so-called Operational Calculus in the Laplace variable s, as detailed in Zehetner et al. (2007); Reger & Jouffroy (2009); Mboup et al. (2009). Indeed, in the ADP the jth-order time-derivative of a signal is computed using the convolution integral

$$y_{\text{adp}}^{(j)}(t) = (-1)^{(j)} \int_0^{T_{\text{adp}}} \Pi_{jN\varpi}(T_{\text{adp}}, \tau) y(t-\tau) d\tau, \tag{4.1}$$

where $y_{\text{adp}}^{(j)} \in \mathbb{R}$ is the ADP estimated jth-order time-derivative of signal $y(t)$, $\Pi_{jN\varpi}(T_{\text{adp}}, \tau)$ is the ADP kernel function, $y(t)$ is the measured and noisy signal which is applied to the ADP; and $T_{\text{adp}} > 0$ is a constant that represents the interval of integration. The tuning of the ADP depends on the selection of T_{adp}, which can be interpreted as the window width of a receding horizon estimation. The specific value of T_{adp} is chosen considering the tradeoff between non-negligible time-delay and better noise rejection as the value of this parameter increases. The general expression for the ADP kernel function is given by (Zehetner et al., 2007)

$$\begin{aligned}\Pi_{jN\varpi}(T_{\text{adp}}, \tau) =& \frac{(N+j+\varpi+1)!(N+1)!(-1)^j}{T_{\text{adp}}^{N+j+\varpi+1}} \times \\ & \sum_{k_1=0}^{N-j} \sum_{k_2=0}^{j} \frac{(T_{\text{adp}}-\tau)^{\varpi+k_1+k_2}(-\tau)^{N-k_1-k_2}}{k_1!k_2!(N-j-k_1)!(j-k_2)!(N-k_1-k_2)!(\varpi+k_1+k_2)!(N-k_1+1)},\end{aligned} \tag{4.2}$$

where j is the order of the time-derivative of the input signal; N is the order of the Taylor expansion (the Taylor polynomial degree); and $\varpi \geq 0$ is an arbitrary nonnegative integer (see (Zehetner et al., 2007, Section II)).

By the trapezoidal numerical integration we can compute an approximation for the ADP integral in (4.1), such that the discrete-time values $y_{\text{adp,d}}^{(j)}(k) = y_{\text{adp}}^{(j)}(kT_{\text{s}})$ are given by

$$y_{\text{adp,d}}^{(j)}(k) \approx (-1)^{(j)} \frac{T_{\text{s}}}{2} \sum_{i=1}^{M} (\Pi_{i-1} y_{k-i+1} + \Pi_i y_{k-i}), \tag{4.3}$$

where $y_{k-i} = y(k-i)T_{\text{s}}$ and $\Pi_i = \Pi_{jN\varpi}(T_{\text{adp}}, iT_{\text{s}})$. The parameter T_{s} is the sampling time used to compute the convolution integral (4.1), and M is the number of integration steps, which can be computed by $M = T_{\text{adp}}/T_{\text{s}}$.

The main idea in the ADP is to compute an approximation of the system's output by means of a polynomial time function with a prescribed degree of nonlinearity N

$$y(\tau) \approx a_0 + a_1\tau + \ldots + a_N\tau^N, \;\; \tau \in [t - T_{\text{adp}}, t],$$

where the coefficients a_i, with $i = 0, 1, 2, \ldots, N$, can be computed using (4.3) with $k = 0$, since, from a truncated Taylor expansion of the signal in time one has that

$$a_0 = y(0), \quad a_1 = y'(0), \quad a_2 = \frac{y^{(2)}(0)}{2!}, \quad \cdots, \quad a_N = \frac{y^{(N)}(0)}{N!}.$$

Interestingly, one of the advantages of the ADP is that the coefficient computation only depends on time integrals, which makes them somewhat robust to noise. Moreover, the ADP is implemented as a linear Finite Impulse Response (FIR) digital filter, and therefore it is Bounded-Input Bounded-Output (BIBO) stable. On the other hand, a disadvantage of the ADP is an unavoidable time-delay in its estimation that depends on the selected T_{adp}.

The ADP has been a derivative estimation technique used in the model-free control strategy proposed by Fliess & Join (2013) for some applications as exemplified in Mohammad Ridha et al. (2015).

Due to the noise rejection property of the ADP, we propose a FIR filter in the TRS' output to smooth out the quantization error and improve the ESO's estimate, as shown in Figure 4.1. The parameters of the ADP kernel function in (4.2) were selected such that $j = 0$ (we are interested in a smooth approximation of the signal itself), $N = 1$ (a first order time polynomial is employed), and $\varpi = 0$. Using this parameters we have that, from (4.1),

$$y^{(0)}_{\text{adp}}(t) = \int_0^{T_{\text{adp}}} \frac{-6\tau + 4T_{\text{adp}}}{T^2_{\text{adp}}} y(t - T_{\text{adp}}) d\tau. \tag{4.4}$$

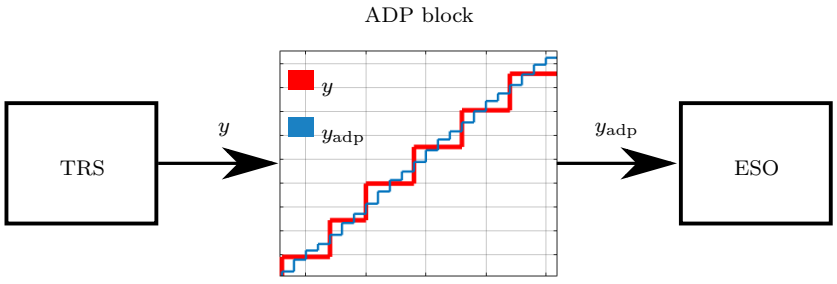

Figure 4.1: ADP function in the TRS.

4.2.2 Robust and Exact Differentiator (RED)

The RED is another time-derivative estimation strategy that employs a sliding mode technique, as shown in Levant (1998), where a controller is designed to achieve $\lim_{t\to\infty}[\chi(t) - \psi(t)] = 0$, with $\chi(t)$ the state of the first-order pure integrator given by $\dot{\chi} = \mu$, and $\chi, \mu \in \mathbb{R}$. Assuming that this control problem fulfills the zero error objective, then the output signal $\mu(t)$ can be used as an estimative of the time-derivative of the signal $\psi(t)$, which

belongs to the space $H[g,h]$ of measurable functions bounded on a segment $[g,h]$ and let $\|\psi\| = \sup|\psi(t)|$ (Levant, 1998).

Note that the *robust and exact differentiator* proposed by Levant (1998) was based on definitions such as: a differentiator is called *exact* on some input $\psi(t)$ if the output coincides with its derivative; a first-order differentiator is called *robust* on some input $\psi(t)$ if the output tends uniformly to $\dot{\psi}(t)$ while the input signal tends uniformly to $\psi(t)$; a differentiator is called *correct* on some input $\psi(t)$ if it is exact and robust on it. These definitions represent a different idea with respect to the current robust and exact differentiator concepts, which can be related to the precision and robustness of a differentiator to deal with parametric uncertainties or disturbances in the input signal.

The control strategy used in the RED is a second-order sliding mode controller (Shtessel et al., 2014; Bartolini et al., 2003), which ensures finite-convergence of the error. The RED subsystem is given by

$$\begin{aligned} \dot{\chi} =& \mu, \\ \dot{\mu}_1 =& -\kappa\,\mathrm{sign}(\chi(t)-\psi(t)), \\ \mu =& \mu_1 - \lambda|\chi(t)-\psi(t)|^{\frac{1}{2}}\,\mathrm{sign}(\chi(t)-\psi(t)), \end{aligned} \tag{4.5}$$

where $\psi(t)$ is the input signal to be differentiated. The scalar parameters λ and κ are obtained using the result in Levant (1998, Theorem 1):

$$\begin{aligned} \kappa >& C, \\ \lambda^2 \geq& 4C\frac{\kappa + C}{\kappa - C}, \end{aligned} \tag{4.6}$$

where C is a Lipschitz constant for $\dot{\psi}(t)$, i.e. the time-derivative of $\psi(t)$ is assumed to satisfy $|\dot{\psi}(t_2) - \dot{\psi}(t_1)| \leq C|t_2 - t_1|$, $\forall t_1, t_2 \in \mathbb{R}$. It is worth noticing that high frequency additive noise can degrade considerably the performance of RED (Levant, 1998).

In order to compute the RED parameters λ and κ for the ID controller described in Section 4.3, we first compute the Lipschitz constant C using the simulated data of the rotational speed of the DC motor obtained from TRS model defined in Chapter 2.

According to Levant (1998, Theorem 1), the Lipschitz constant C for the TRS must satisfy $|\omega(t_2) - \omega(t_1)| \leq C_1|t_2 - t_1|, \forall t_1, t_2$, and $|\dot{\omega}(t_2) - \dot{\omega}(t_1)| \leq C_2|t_2 - t_1|, \forall t_1, t_2$, which was verified through of the polynomial regression given by

$$\omega(t) = 0.0048881t^5 - 0.079944t^4 + 0.52029t^3 - 1.7194t^2 + 2.9863t + 0.022921,$$

and its time-derivative polynomial equation given by

$$\dot{\omega}(t) = 0.0244t^4 - 0.3198t^3 + 1.5609t^2 - 3.4388t + 2.9863.$$

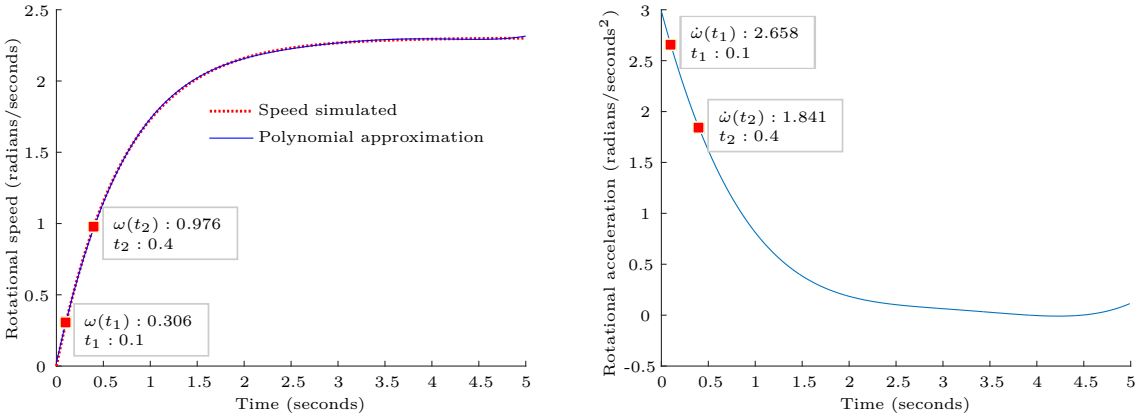

(a) Polinomial regression. (b) Time-derivative of the polynomial.

Figure 4.2: Simulated data used to compute the Lipschitz's constant of the TRS.

For the polynomial regression it was used a step signal of 2.1 volts in the input of the DC motor of the TRS in open loop, during 5 seconds. Figure 4.2 shows the points used to compute $C_1 = 2.26$ and $C_2 = 2.72$ for the polynomial regression and its time-derivative, respectively. The highest value of Lipschitz constant C was used for the selection of the RED parameters κ and λ, considering (4.6). In addition to the fulfillment of the established parameters conditions, we consider a selection by simulated results, where initially, it is chosen κ with the best result using the equal symbol in the condition to compute λ. Later it is performed a fine tunning with different values of λ that satisfies the conditions. This process was used as criterion to achieve the RED parameters given by

$$\kappa = 6,$$
$$\lambda = 7.1.$$

Note that the rotational speed simulation and the polynomial regression provide an alternative solution to compute the Lipschitz constant of the TRS, since the system does not have a rotational speed and acceleration sensors for the DC motor. However, this still has no guarantee that the Lipschitz constant of the real signal will meet this one, since this is just an estimation.

4.3 The Modified ADRC Strategy

This section presents the modified ADRC strategy applied to the TRS, which employs the two time derivative estimation methods shown in earlier sections. From the original ADRC shown in Figure 3.2, we have that the modifications are added between the ADRC output u and TRS voltage input u_v, and between the TRS output y and the ESO input y_{adp} represented in blue blocks in Figure 4.3. This modifications are called *Algebraic Differentiation Procedure* (ADP) and *Inverse Dynamics* (ID), respectively.

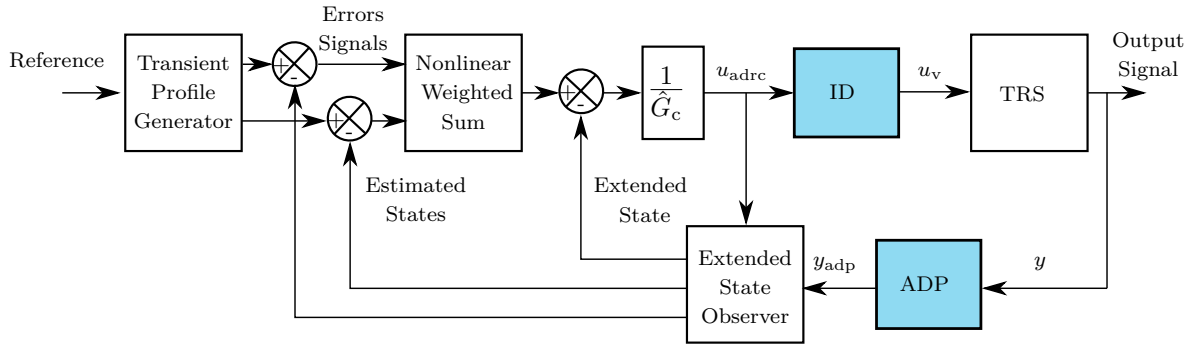

Figure 4.3: Modified ADRC topology. ID ad ADP blocks (blue blocks) are the novel elements.

Note that the modified ADRC uses two differentiator methods: the ADP and the RED contained in the ID. The ADP is used to reject the output quantization of a system, and the RED is used in the ID to obtain a fast time-derivative estimation of the rotational speed from the ADRC control signal. Observe that the ADP could introduce a time delay if used instead of the RED, and the RED could affect the control performance if used instead of the ADP. This is because the ADP could not be fast enough and the RED is very sensitive to high frequency noise.

The ADP is employed to provide a differentiable approximation of the system's output to the ESO input, since the quantization of the system's output signal introduces high frequency content associated with abrupt changes in the measured variables. In the case of the twin-rotor system, this is a consequence of using the incremental encoder to measure the pitch angle. As commented in the previous section, the ADP is denoted by the equation (4.1) and its approximation by the trapezoidal integration (4.3), using the ADP kernel function computed as shown in (4.4). Thus, the discrete-time ADP equation for the TRS is given by

$$y^{(j)}_{\mathrm{adp,d}}(k) \approx \frac{T_\mathrm{s}}{2}\sum_{i=1}^{M}(\Pi_{i-1}y_{k-i+1} + \Pi_i y_{k-i}), \tag{4.7}$$

where the sampling time is $T_\mathrm{s} = 0.01$ seconds, $M = T_\mathrm{adp}/T_\mathrm{s}$, with $T_\mathrm{adp} = 0.2$ seconds, such that $M = 20$, and with $j = 0$, $N = 1$ and $\varpi = 0$, we have that

$$\Pi_i = \Pi_{jN\varpi}(T_\mathrm{adp}, t_i) = \frac{-6t_i + 4T_\mathrm{adp}}{T^2_\mathrm{adp}}. \tag{4.8}$$

On the other hand, the ID scheme is used to drive indirectly the TRS propulsive torque. This is accomplished by computing the necessary input voltage to be applied to TRS main rotor in order to achieve a desired rotational speed associated with a desired propulsion torque $T^\mathrm{d}_\mathrm{p}(t)$, which is provided by the ADRC strategy. Thus the TRS, thanks to this inverse dynamics based scheme, is seen by the ADRC controller as a second-order system.

From the propulsion torque equation (2.5) and considering that the state-space variable

x_3 represents the rotational speed ω, yields $T_{\mathrm{p}}(x_3) = T_{\mathrm{p}}^{\mathrm{d}}(t)$ at every time instant. In this case, one can compute only the positive value $x_3^{\mathrm{d}}(t)$ that satisfies the polynomial equation $T_{\mathrm{p}}^{\mathrm{d}}(t) = \alpha_1(x_3^{\mathrm{d}}(t))^2 + \alpha_2 x_3^{\mathrm{d}}(t)$, such that a desired reference value $x_3^{\mathrm{d}}(t)$ is obtained:

$$x_3^{\mathrm{d}}(t) = \frac{-\alpha_2 + \sqrt{{\alpha_2}^2 + 4\alpha_1 T_{\mathrm{p}}^{\mathrm{d}}(t)}}{2\alpha_1}. \tag{4.9}$$

Using the DC motor equation (2.6), the input voltage $u_{\mathrm{v}}(t)$ can be computed by relying on the time-derivative estimation $\mu(t)$ of the signal $x_3^{\mathrm{d}}(t)$ in (4.9) obtained from the RED such that

$$u_{\mathrm{v}}(t) = \frac{1}{k_{\mathrm{m}}}\left[\tau_{\mathrm{m}}\mu(t) + x_3^{\mathrm{d}}(t)\right], \tag{4.10}$$

where the time-derivative estimation $\mu(t)$ in computed using $\kappa = 6$ and $\lambda = 7.1$. The ID scheme is shown in Figure 4.4, with $u = T_{\mathrm{p}}^{\mathrm{d}}(t)$ and the parameters α_1, α_2, τ_{m} and k_{m} have the same values defined in Section 2.4.

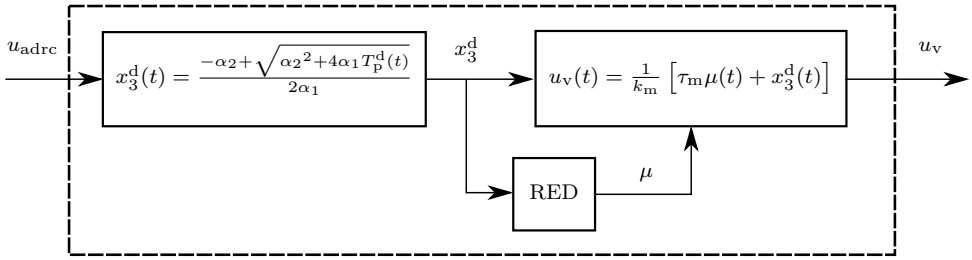

Figure 4.4: Inverse Dynamics scheme.

It is important to note that assuming the time-derivative estimation given by the RED $\mu(t) = \dot{x}_3^{\mathrm{d}}(t)$ and considering $\tau_{\mathrm{m}} > 0$ positive constant, we can guarantee that (4.10) leads to $\lim_{t\to\infty} x_3 - x_3^{\mathrm{d}} = 0$, i.e. the asymptotic tracking of the desired angular speed will be achieved. Using the DC motor model (2.6) and substituting $u_{\mathrm{v}}(t)$ from (4.10) the following is obtained

$$\begin{aligned}
\tau_{\mathrm{m}}\dot{x}_3(t) &= -x_3(t) + k_{\mathrm{m}}\left(\frac{1}{k_{\mathrm{m}}}\left(\tau_{\mathrm{m}}\dot{x}_3^{\mathrm{d}}(t) + x_3^{\mathrm{d}}(t)\right)\right), \\
\dot{x}_3(t) - \dot{x}_3^{\mathrm{d}}(t) &= -\frac{1}{\tau_{\mathrm{m}}}\left(x_3(t) - x_3^{\mathrm{d}}(t)\right), \\
\dot{e}_{\mathrm{id}} &= -\frac{1}{\tau_{\mathrm{m}}}e_{\mathrm{id}},
\end{aligned} \tag{4.11}$$

where the error is denoted by $e_{\mathrm{id}} = x_3(t) - x_3^{\mathrm{d}}(t)$. The solution of (4.11) guarantees that $\lim_{t\to\infty} x_3 - x_3^{\mathrm{d}} = 0$ with $\tau_{\mathrm{m}} > 0$, which is given by

$$e_{\mathrm{id}} = e_{\mathrm{id0}}e^{\left(-\frac{t}{\tau_{\mathrm{m}}}\right)},$$

where e_{id0} is an initial value and t is the time response of the TRS mechanical dynamics.

It is worthwhile to mention that the dynamical cancellation can work in the control of the TRS, and the decay rate of this error will be equal to $5\tau_{\mathrm{m}}$. In other words, to ensure that error convergence decayed to zero, $5\tau_{\mathrm{m}}$ must be much smaller than the time response of the TRS mechanical dynamics.

Note that, although the approximated dynamical cancellation in Figure 4.4 is not robust to parametric uncertainties in the DC motor parameters, by relying on the claimed robustness of the ADRC strategy, one expects to still have good results.

4.4 Simulation Results

This section presents the simulation results of the controllers based on the ADRC strategy applied to the TRS. In this approach, it is desired to control the pitch angle of the TRS, as shown in Figure 2.1. Using the block diagram of Chapters 3 and 4, we proposed four ADRCs strategies – two pure and two modified – which are used in this section. Furthermore, the quantitative and qualitative results of the control effort and tracking error are presented. The simulations were carried out in the MATLAB/Simulink® environment, using the TRS model and the parameters defined in the Section 2.4.

All ADRC strategies used in the simulations were defined with nonlinear observer gains given by (3.5) and linear control gains. In order to present the results, the simulations were organized in three groups as shown in Table 4.1, where two cases of pure ADRCs are used, one is named ADRC(3) because it uses an ESO that estimates three states including the extended state, and the other one is named ADRC(4) because its ESO estimates four states; also two modified ADRC are used, one is named ADRC ID because it is a version of the ADRC(3) with an inverse dynamics scheme, and the other one is named ADRC ID ADP due to a version of the ADRC ID with an algebraic differentiation procedure. The controllers are tested with two TRS models, one is the complete TRS model (2.7) and the other one is the simplified version of the TRS model[1] (2.2).

Simulation groups	**Controllers**				**TRS model**
	ADRC(3)	ADRC(4)	ADRC ID	ADRC ID ADP	
1	X	X			Complete
2	X	X			Simplified
3			X	X	Complete

Table 4.1: Organization of the controllers and the TRS models used in the simulation test.

For each simulation group, the simulation time has been set to 60 seconds and the chosen integration method was a fixed-step Runge-Kutta (Davis & Rabinowitz, 2007), with a sampling time of 0.01 seconds. Additionally, in order to evaluate the attitude regulation and the tracking of the time-varying reference of the controllers in each simulation group,

[1]The simplified TRS model considers the propulsion torque as input.

we used two types of reference signals: one was a step with amplitude of 0.5981 and initial time of 5 seconds, the other one was a sinusoidal curve with amplitude of 1.0472 radians peak to peak, bias of 0.5236 radians, and period of 30 seconds.

In order to compare the simulation results of the output system, we used the signal obtained by the transient profile generator (3.2) as reference, with a smoothing parameter $p_{\mathrm{s}} = 0.1$, which is chosen in order to obtain a smooth reference and improve the closed-loop system behavior.

In Section 4.4.1, the results of each simulation group are presented.

4.4.1 Pure ADRC Strategies with TRS Model

The block diagram for the first group with pure ADRCs is shown in Figure 3.2, where the plant is the TRS with input as voltage signal and output as the pitch angle, as described in the Section 2.4. For the ADRC(3) case, the ESO estimates three states, therefore the observer gains are computed considering (3.11), where the real part of the eigenvalues in this expression are allocated around -10. This choice comes from the smoothing behavior of the ADRC. However, similarly to the linear control design, the observer dynamics – given by the eigenvalues – must be faster than the controller dynamics. Using (3.27) we computed the control gains, where the real part of the eigenvalues in the later expression are allocated around -0.7, which ensure stability of the closed-loop system, and also, that the control dynamics – given by the eigenvalues – is slower than the observer dynamics. Thereby, for the ADRC(3) control law (3.7), we defined $\hat{G}_{\mathrm{c}} = \frac{1}{I_{\mathrm{h}}} = 14.2450$, and for (3.8) we chose the control gains $K_{\mathrm{p}} = 4.5$ and $K_{\mathrm{d}} = 1.5$. For the ESO (3.6), we considered the functions $\ell_1(x_1 - \hat{x}_1) = L_1(\tilde{x}_1)$, $\ell_2(x_1 - \hat{x}_1) = L_2 f_1(\tilde{x}_1, 0.5, \varrho)$, $\ell_3(x_1 - \hat{x}_1) = L_3 f_2(\tilde{x}_1, 0.25, \varrho)$, according to (3.5), with the observer gains defined as $L_1 = 28.8881$, $L_2 = 278.0063$ and $L_3 = 891.8834$, and $\varrho = 1$.

For the ADRC(4) case, we have an ESO that estimates four states, thus to compute the observer gain we used (3.11) with an additional state and the same criterion to allocate it used in ADRC(3), with the real part of the eigenvalues around -10. The control gains were tuned considering the derivative control gain should not be too large because this has a notable effect in the control dynamics. Thereby, for the ADRC(4) control law (3.7), we defined $\hat{G}_{\mathrm{c}} = 14.2450$, and for (3.8) we chose the control gains $K_{\mathrm{p}} = 8$ and $K_{\mathrm{d}} = 1.5$. For the ESO (3.6) with an additional state, we considered the functions $\ell_1(x_1 - \hat{x}_1) = L_1(\tilde{x}_1)$, $\ell_2(x_1 - \hat{x}_1) = L_2 f_1(\tilde{x}_1, 0.5, \varrho)$, $\ell_3(x_1 - \hat{x}_1) = L_3 f_2(\tilde{x}_1, 0.25, \varrho)$, $\ell_4(x_1 - \hat{x}_1) = L_4 f_3(\tilde{x}_1, 0.25, \varrho)$; with observer gains defined as $L_1 = 36.7$, $L_2 = 505.3$, $L_3 = 3093.4$ and $L_4 = 7103.1$, and $\varrho = 1$.

The simulation results of the first group of pure ADRCs with a step reference are shown in Figure 4.5.

In Figure 4.5, one can observe that both pure ADRCs converged to the desired reference, although both strategies present a time-delay due to the observer dynamics. Moreover,

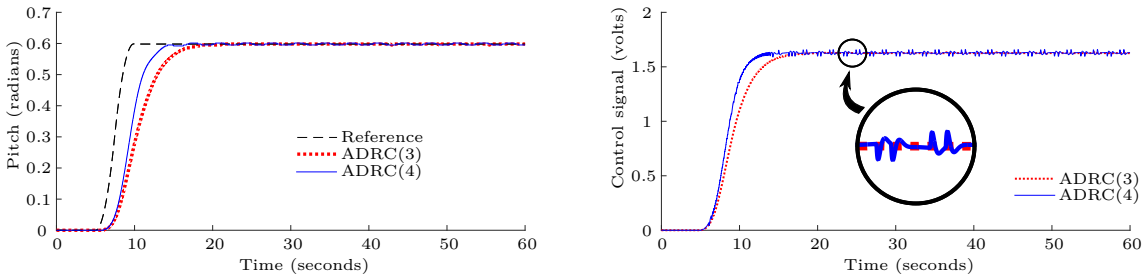

(a) Simulation Results. (b) Control Signal.

Figure 4.5: Simulation results of the first group using a step reference.

since the ADRC(4) was tuned to be aggressive, its raising time is faster, but the control effort was larger with some jitter in steady state due to the quantized output of the TRS.

With the purpose of evaluating the first group of pure ADRCs with a time-varying reference, it was used a sinusoidal reference as shown in Figure 4.6.

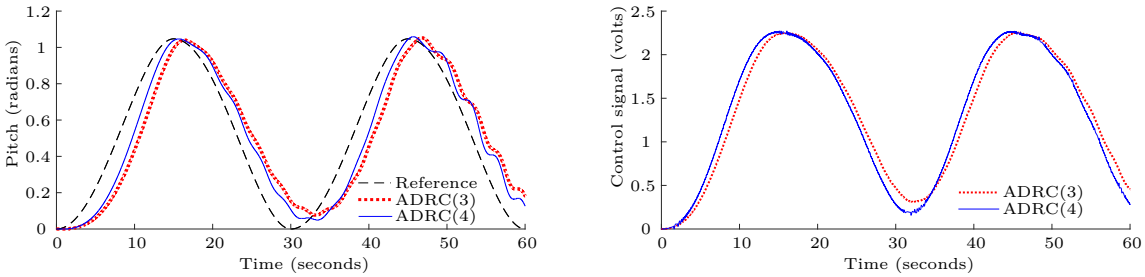

(a) Simulation Results. (b) Control Signal.

Figure 4.6: Simulation results of the first group using a sinusoidal reference.

In Figure 4.6 it is observed that both strategies initially present a significant time-delay with respect to the reference, followed by an increase of ripples in the output signal. Thereby, none of the pure ADRC strategies were able to track a time-varying reference.

4.4.2 Pure ADRC Strategies with the Simplified TRS Model

Similar to the first simulation group, the block diagram used in the second group with the pure ADRCs is shown in Figure 3.2. Since the simulation environment allows modifications in the TRS model, we were able to test a possible solution to control the TRS using a simplified representation of the TRS model. Assuming that the input in the TRS is the torque propulsion, the third order model (2.7) described in the Section 2.4, is used as was shown in (2.2). Thereby, the simplified system used to formulate the ADRC strategy is

given by

$$\begin{aligned}\dot{x}_1 &= x_2,\\ \dot{x}_2 &= \underbrace{\left(-\frac{1}{I_\mathrm{h}} m_\mathrm{g} \sin(x_1) - \frac{1}{I_\mathrm{h}} b_\mathrm{f} x_2\right)}_{F(t)} + \underbrace{\left(\frac{1}{I_\mathrm{h}}\right)}_{G(t)} \underbrace{T_\mathrm{p}}_{u}.\end{aligned}$$

The ADRC formulation for the simplified TRS model is simply given by (3.1), shown in Section 3.1. It is important to mention that the value $\hat{G}_\mathrm{c} = \frac{1}{I_\mathrm{h}}$ is used in all tests.

Similar to the first simulation group, the linear control gains and the nonlinear observer gains of the pure ADRC strategies – ADRC(3) and ADRC(4) – are computed such that the control and the observer gains obtained are equal to the values obtained to the pure ADRCs in the first group.

The simulation results for the second group of pure ADRC strategies with the simplified TRS model are shown in Figure 4.7, where the reference is a step signal. Since the results for the ADRC(4) have larger variations, as depicted in (a) and (b), only the results of ADRC(3) are shown in (c) and (d).

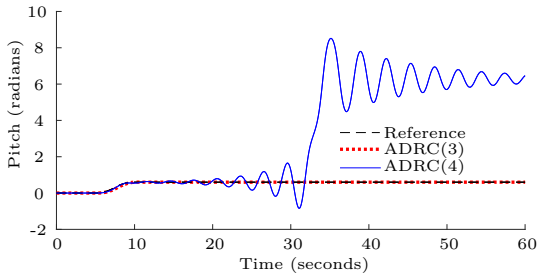

(a) Simulation Results of ADRC(3) and ADRC(4).

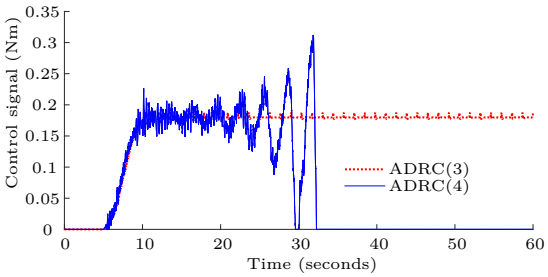

(b) Control Signal of ADRC(3) and ADRC(4).

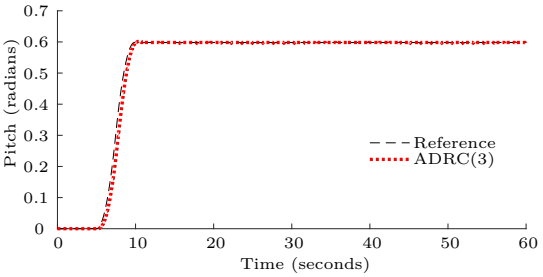

(c) Simulation Results of ADRC(3).

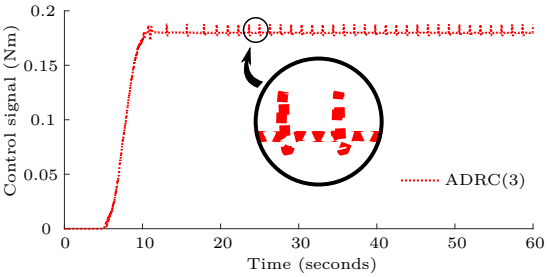

(d) Control Signal of ADRC(3).

Figure 4.7: Simulation results of the second group using a step reference.

In Figure 4.7, one can observe that initially both controllers track the step reference, but the ADRC(4) begins to accumulate ripples until completely destabilize the simplified TRS model. On other hand, the ADRC(3) is able to keep stable the simplified TRS model, and additionally, it successfully tracks the step response, with minor variations in steady state due to effect of the quantization error in the output of the TRS.

The simulation results obtained in the case where a sinusoidal reference is applied in

the second group of the pure ADRCs are shown in Figure 4.8. Since the results for the ADRC(4) have larger variations, as depicted in (a) and (b), only the results of ADRC(3) are shown in (c) and (d).

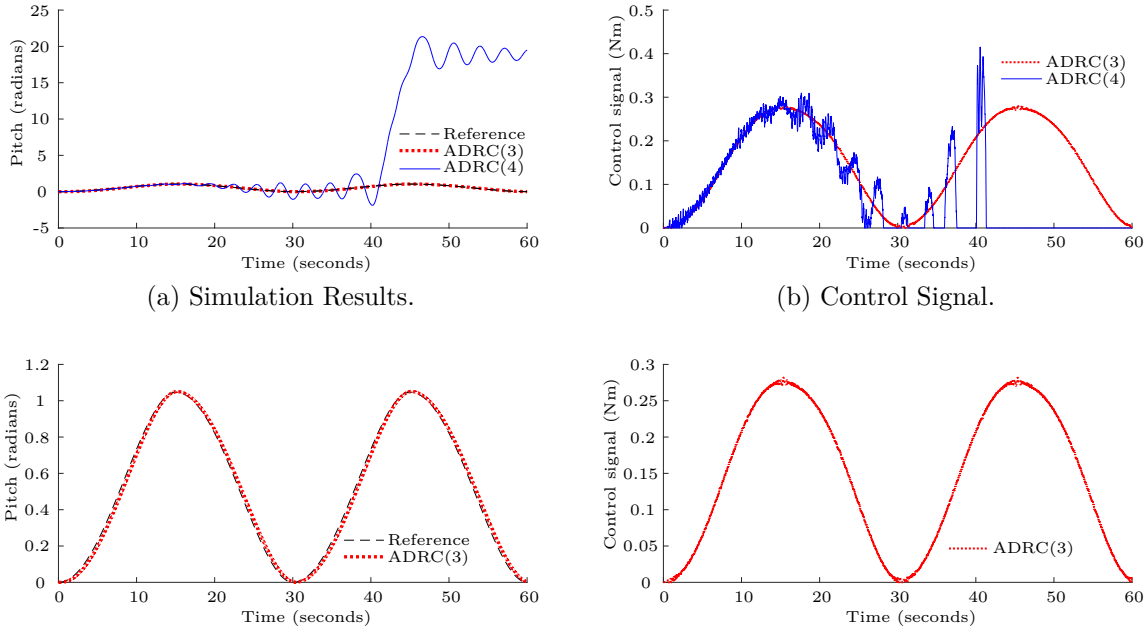

(a) Simulation Results.

(b) Control Signal.

(c) Simulation Results.

(d) Control Signal.

Figure 4.8: Simulation results of the second group using a sinusoidal reference.

In Figure 4.8, it is observed that initially both control strategies are tracking the sinusoidal reference, but the ADRC(4) begins to accumulate ripples until completely destabilize the simplified TRS model again. On the other hand, the ADRC(3) presents a good performance, maintaining stable the simplified TRS and successfully tracking the sinusoidal reference, with a noiseless control signal.

With the simulation results obtained for the second group, we can conclude that the structure of the ADRC(3) allows a suitable nonlinear cancellation in order to control the simplified TRS model.

4.4.3 Modified ADRC Strategies with TRS Model

This section presents the simulation results obtained by the third group of modified ADRC strategies, which is represented by a block diagram, as shown in Figure 4.3. Similar to the first simulation group, the TRS model (2.7) has the voltage as input signal and the pitch angle measure as output, as described in Section 2.4. Based on the successful simulation results of ADRC(3) obtained in the second group, we proposed a modified ADRC, which used the same nonlinear observer gains and the linear control gains of the ADRC(3) from the first group, and additionally, the modified ADRC includes the inverse dynamics scheme to make the TRS model (2.7) behave as the simplified TRS model.

In order to show the improvement of the simulation results in the modified ADRC with ADP, we used two modified ADRCs: the ADRC ID and the ADRC ID ADP. To carry out the analysis, first it is presented the graphic results followed by a quantitative comparison of error and control effort.

The simulation results of the third group of modified ADRCs using a step reference are shown in Figure 4.9.

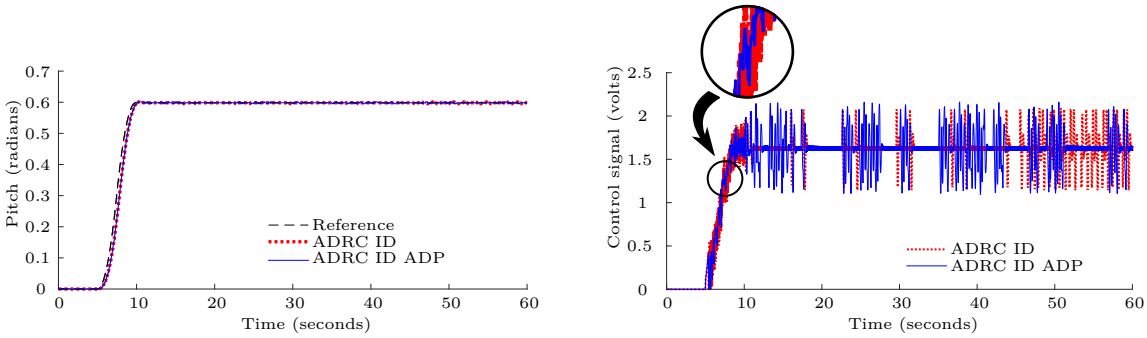

(a) Simulation Results. (b) Control Signal.

Figure 4.9: Simulation results of the third group using a step reference.

In Figure 4.9, one can observe that both modified controllers achieved a good performance in the step response, maintaining stable the TRS. Furthermore, the time-delay introduced by the observer dynamics was reduced. On the other hand, the results of the control signals showed that there is a small difference in the control effort between the ADRC ID and the ADRC ID ADP, where the ADRC ID ADP is the strategy that presented less control effort. This is due to fact that the ADP is able to smooth the quantization error effect of the TRS output to the ESO input. However, the control signal still presents a chattering in the steady state due to quantization effect.

Finally, the simulation results of the third group of the modified ADRCs in closed-loop with TRS model are shown in Figure 4.10, where the tracking of a sinusoidal reference is obtained.

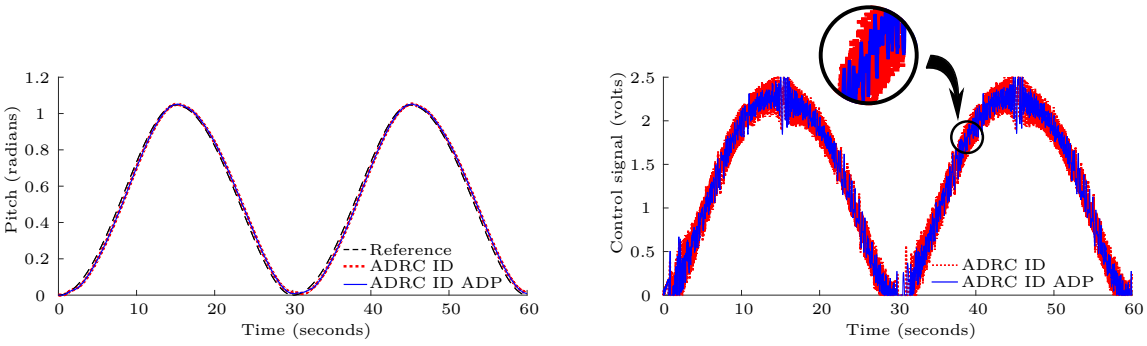

(a) Simulation Results. (b) Control Signal.

Figure 4.10: Simulation results of the third group using a sinusoidal reference.

Figure 4.10 illustrates that both modified ADRC controllers were able to track the sinusoidal reference, maintaining stable the TRS throughout the desired trajectory. Also, the ADRC ID ADP presented the lowest control effort.

Considering that the best simulation results were obtained by the modified ADRCs and the sinusoidal signal is a suitable reference to evaluate the control attitude in the TRS, we performed a quantitative analysis of the results depicted in Figure 4.10, which is shown in Table 4.2. The indexes used in the quantitative analysis were three: the Integral of the Absolute Derivative of the Control signal (IADU) given by (4.12), which measures of control signal effort u over the simulation time; the Integral of the Squared Error (ISE) given by (4.13), which is an index of error e between the reference and the output system; and the Integral of the Time-weighted Absolute Error (ITAE), computed as shown in (4.14), which is an index of error e between the reference and the output system considering the simulation time.

$$IADU = \int_0^\infty \left| \frac{du(t)}{dt} \right| dt. \tag{4.12}$$

$$ISE = \int_0^\infty e(t)^2 dt. \tag{4.13}$$

$$ITAE = \int_0^\infty t\,|e(t)|\,dt. \tag{4.14}$$

Performance of the controllers		
Metrics of the control signal		
Metric	ADRC ID	ADRC ID ADP
IADU	707.7638	193.1487
Error between reference and output system		
Metric	ADRC ID	ADRC ID ADP
ISE	0.0362	0.0358
ITAE	40.5292	39.922

Table 4.2: Performance indexes of the modified ADRCs in the simulation results.

From Table 4.2 we have that both modified ADRC controllers present similar tracking response, since the computed ISE and ITAE are almost the same. However, as highlighted before, the control effort spent by the modified ADRC, taking into account the ADP technique, is significantly reduced, as shown by the IADU index. Considering that in a control design it is desired a low power consumption, the ADP in the modified ADRC allows to achieve better results when the system's output is quantized.

4.5 Final Remarks

This chapter presented the main motivations to elaborate the modifications of the original ADRC. The quantization output is one of the TRS issues that in the ADRC strategy generates an estimation error in ESO and consequently a greater control signal effort. By adding the ADP to the ESO input, the quantization effect is decreased and, consequently, the control signal effort also decreases, as shown in the simulation results of the third controller group. The dynamics of a third order system is another TRS issue that affect the performance of the original ADRC, because the ADRC formulation is designed to control a second-order nonlinear system with full relative degree. In order to improve the control attitude of the ADRC with TRS considering the preview issue, the original ADRC structure was modified, by adding an ID scheme between the ADRC output and the TRS input. The ID scheme in the modified ADRC cancels the dynamics and the system successfully tracks the reference, as show in the third controller group in simulation results.

Simulation results were obtained in the MATLAB/Simulink® environment, where the TRS model described in the Section 2.4 was used, considering that in the model the movement of the DC motor is restricted to only one direction. The controllers applied in the simulations were organized in three groups: the first group consist of the pure ADRC strategies ADRC(3) and ADRC(4) with the TRS model; the second group consist of the pure ADRC controllers ADRC(3) and ADRC(4) with a simplified TRS model; and the third group consists of the modified ADRC controllers ADRC ID and ADRC ID ADP with the TRS model.

Simulation results of the first group of pure ADRCs showed that both controllers were able to stabilize the TRS when a step reference is used. However, in the transient stage the time-delay of the output system was significant. On the other hand, when a sinusoidal reference is used, both controllers showed initially a time-delay when tracking the reference with incremental ripples that accumulate up to total failure of the TRS.

In the second group of pure ADRCs, we simplified the TRS model and tested the performance of the controllers. The simulation results obtained showed that the ADRC(4) controller destabilized the simplified TRS model for the two types of references used. On the other hand, the ADRC(3) controller successfully tracked the two references with the simplified TRS model. Thereby, considering the successful results obtained with the simplified TRS model and ADRC(3), we proposed the third group of modified ADRC controller where the ADRC(3) is used with an additional inverse dynamics scheme, which was formulated to cancel the dynamics of the TRS model so that it behaves like the simplified TRS model.

Finally, the simulation results obtained for the third group of modified ADRCs in closed-loop with the TRS model showed that both controllers successfully tracked the reference

signals. Additionally, the quantitative analysis corroborates the better performance of the ADRC ID ADP when compared with the ADRC ID, mainly due to the lower control signal power consumption by the ADRC ID ADP.

5 Experimental Results

In the previous chapter, the modified ADRC strategy was presented along with its main motivations, a description of the two additional schemes adjusted to the TRS model, and the simulation results obtained in the MATLAB/Simulink® environment. Furthermore, the simulation results have shown a successful performance of the modified ADRC ID ADP control strategy.

In order to evaluate the performance of the controller presented in Chapters 3 and 4, this chapter shows the experimental results obtained in a real Twin-Rotor system using two controller groups: the pure ADRCs and the modified ADRCs. The purpose of the experiments is to evaluate the controller performance in a step response and tracking of a sinusoidal signal, as shown in Section 4.4. Also, a qualitative and quantitative analysis of the experimental results obtained when controlling the TRS by the original ADRC and the modified ADRC are presented.

This chapter is organized as follows: Section 5.1 shows the equipments and details considered in the experimental setup; Section 5.2 describes the procedure performed in each test; and finally, Section 5.3 presents the results obtained followed by a quantitative analysis to evaluate the performance of the controllers.

5.1 The Experimental Setup

To carry out the experiments, the Twin-Rotor Multiple-Input Multiple-Output (MIMO) system 33-220 manufactured by the Feedback Instruments was used (Figure 5.1). Seeking

to control only the pitch movements, the plastic locking screw is tightened to eliminate yaw movements, leaving the TRS with only one-degree of freedom.

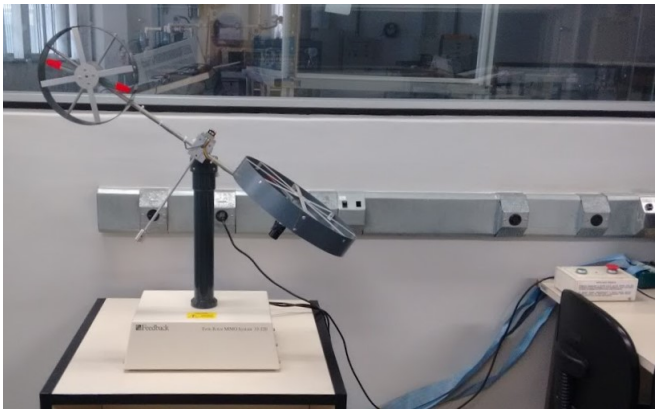

Figure 5.1: Real TRS.

According to the manual (Feedback, 2006), the experimental equipment required to use TRS consists of:

- Twin-Rotor MIMO system - mechanical and electronic units;
- A remote on/off switch box for the Twin-Rotor MIMO system;
- PC with a PCL1711 card;
- Feedback Cable Adapter box.

Figure 5.2 shows the complete experimental setup at the control laboratory of the Universidade Federal de Minas Gerais.

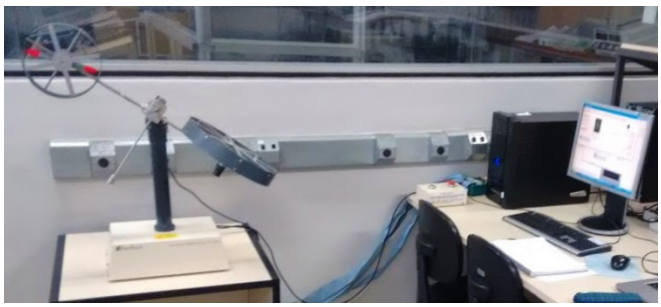

Figure 5.2: Control system of real TRS.

The computer used in the experiment runs Windows XP operating system, MATLAB/Simulink® version 7.4 (R2007a), and the drivers of Advantech PCL1711 card. The Twin-Rotor MIMO system software was used to control and acquire measurements of the TRS in real time.

5.2 Test Description

This section describes the experimental test procedure and its technical details, such as: sample time, reference signals, and controllers. Similar to Section 4.4, four controllers were used: two pure ADRCs – ADRC(3) and ADRC(4) – and two modified ADRCs – ADRC ID and ADRC ID ADP.

The experimental results were organized in three groups: the first group consists of pure ADRC controllers in close-loop with the real TRS; the second group consists of modified ADRC controllers in close-loop with the real TRS; and finally, in the third group the modified ADRCs are also used, and their ability to reject disturbance in closed-loop with real TRS was evaluated with the introduction of a step disturbance.

All experimental tests have been set to take 60 seconds, with sampling time equal to 0.01 seconds. The reference signals were generated using the transient profile generator (3.2), with a smoothing parameter $p_{\mathrm{s}} = 0.1$.

The setting of each experimental group are defined as follows:

- For the first experimental group of pure ADRC controllers, the same block diagram presented in Chapter 3 was used, as depicted in Figure 5.3, which explicitly highlights the processes being executed in software with the label "PC". In order to evaluate the step response of the controllers, we used a step reference with amplitude of 0.5981 and initial time of 5 seconds. To evaluate the tracking performance of the controllers, a sinusoidal reference was used with an amplitude of 1.0472 radians peak to peak, bias of 0.5236 radians, and a period of 30 seconds. Thereby, for each controller, two experimental tests were executed using the aforementioned reference signals.

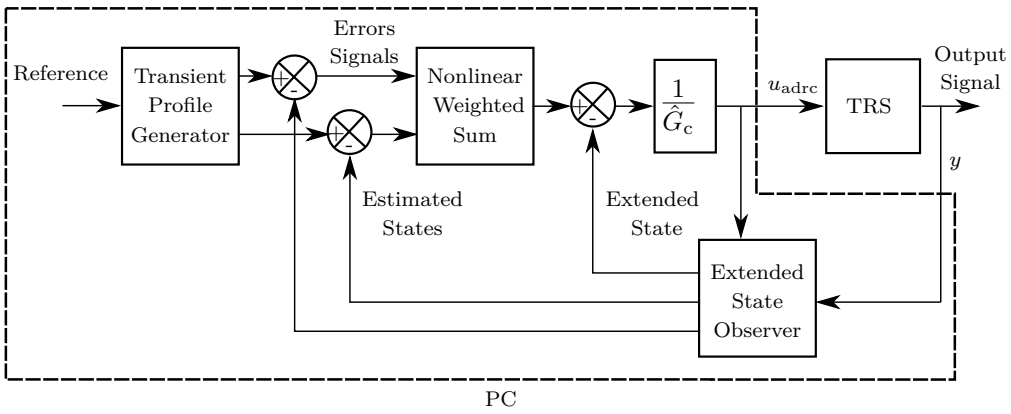

Figure 5.3: Pure ADRC topology.

The controllers' parameters for the first experimental group were chosen in the same way as for the pure ADRCs presented in Section 4.4. Therefore, for the ADRC(3) control law, we defined $\hat{G}_{\mathrm{c}} = 14.2450$, and for its virtual control law we chose the linear gains $K_{\mathrm{p}} = 4.5$ and $K_{\mathrm{d}} = 1.5$. For its ESO we considered the nonlinear functions $\ell_1(y - \hat{x}_1) = L_1(y - \hat{x}_1)$, $\ell_2(y - \hat{x}_1) = L_2 f_1(y - \hat{x}_1, 0.5, \varrho)$, $\ell_3(y - \hat{x}_1) = L_3 f_2(y - \hat{x}_1, 0.25, \varrho)$,

from (3.5) with $\varrho = 1$, and the observer gains defined as $L_1 = 28.8881$, $L_2 = 278.0063$ and $L_3 = 891.8834$.

For the control law ADRC(4), we defined $\hat{G}_c = 14.2450$. For its virtual control law we chose the linear gains $K_p = 8$ and $K_d = 1.5$. For its ESO we considered the nonlinear functions $\ell_1(y - \hat{x}_1) = L_1(y - \hat{x}_1)$, $\ell_2(y - \hat{x}_1) = L_2 f_1(y - \hat{x}_1, 0.5, \varrho)$, $\ell_3(y - \hat{x}_1) = L_3 f_2(y - \hat{x}_1, 0.25, \varrho)$, $\ell_4(y - \hat{x}_1) = L_4 f_3(y - \hat{x}_1, 0.25, \varrho)$, from (3.5) with $\varrho = 1$, and observer gains defined as $L_1 = 36.7$, $L_2 = 505.3$, $L_3 = 3093.4$ and $L_4 = 7103.1$.

- In the second experimental group of the modified ADRC controllers, the same block diagram from Chapter 4 was used, as shown in Figure 5.4, which explicitly highlights the processes being executed in software with the label "PC". In order to evaluate the controllers, the same reference signals described in the first experimental group are used.

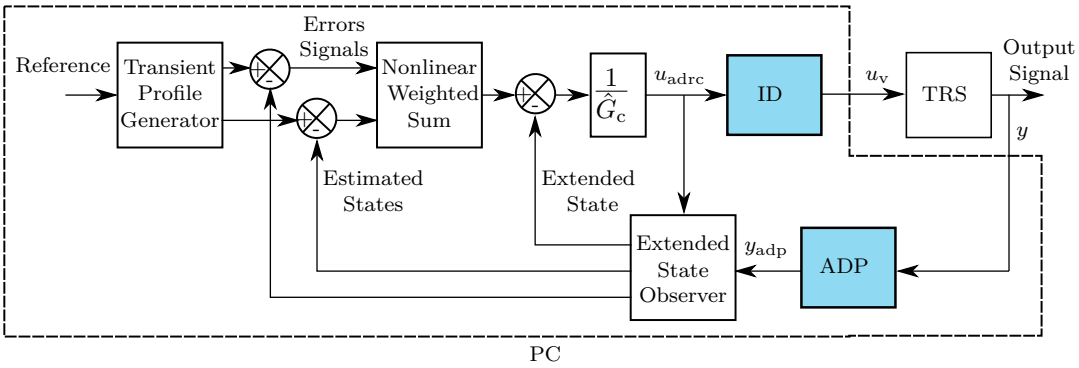

Figure 5.4: Modified ADRC topology.

The modified ADRCs used in this second experimental group are based on the ADRC(3), hence the ADRC parameters are the same ones defined in the first experimental group. Thus, the modified ADRC ID used the ADRC(3) parameters and the ID scheme parameters are defined in Section 2.4, such that $\alpha_1 = 0.0152\,\mathrm{Nm/(rad/s)^2}$, $\alpha_2 = 0.0738\,\mathrm{Nm/(rad/s)}$, $\tau_m = 0.7185\,\mathrm{s}$, and $k_m = 1.0965\,\mathrm{(rad/s)/V}$. The RED block in the ID scheme (see Figure 4.4) and given by the equation (4.5) has been tuned with parameters $\kappa = 6$ and $\lambda = 7.1$.

The modified ADRC ID ADP used the ADRC(3) parameters, the ID parameters defined in the previous controller and the ADP parameters $T_{adp} = 0.2$ and $m = 20$ (see equation (4.7) with the kernel (4.8) defined in Section 4.3).

- Section 5.3 shows that the controllers with best performance are the modified ADRCs. Therefore, these controllers are used again in this third experimental group in a step response evaluation. During the test, it is introduced a step disturbance in the system as shown in Figure 5.5, which is defined with amplitude of 0.5V and initial time at $t = 35$ seconds. This test is used to evaluate the controllers' ability to reject disturbance in closed-loop with the real TRS.

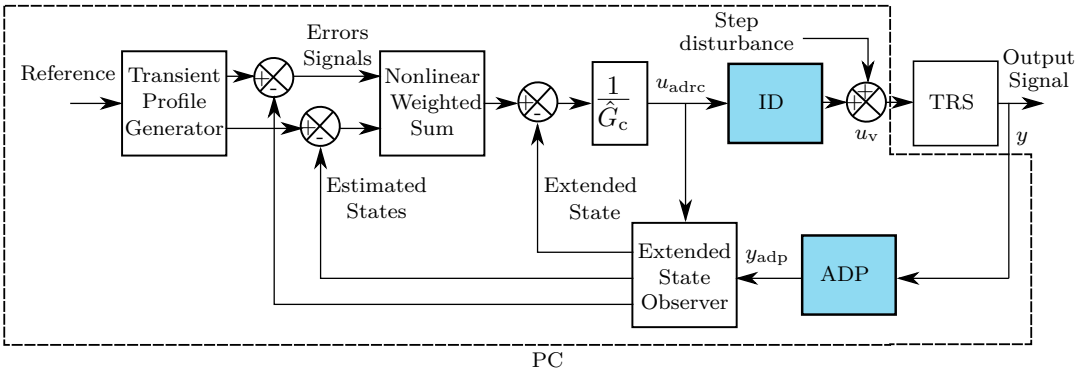

Figure 5.5: Modified ADRC topology with a step disturbance.

5.3 Obtained Results

According to the test description in Section 5.2, the experimental results obtained are presented in the following subsections.

5.3.1 Pure ADRC Strategies with Real TRS

The step responses of the first group of pure ADRCs are shown in Figure 5.6.

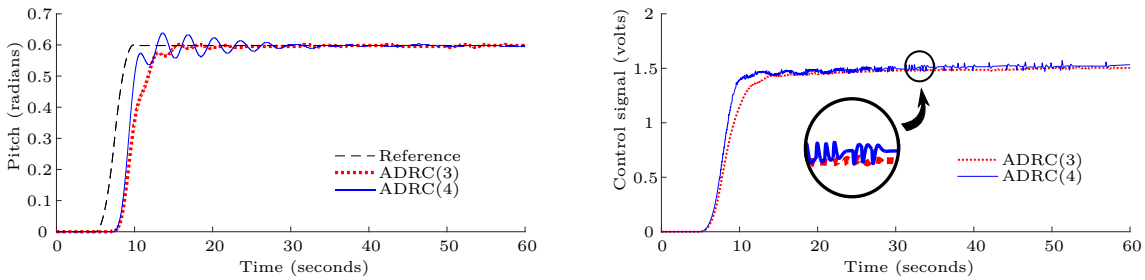

(a) Simulation Results. (b) Control Signal.

Figure 5.6: Step responses of the first group.

In Figure 5.6a, one can observe that both pure ADRC strategies converge to the desired reference, in spite of a time-delay that can be observed in both controllers,which is due to the fact that the ESO dynamics does not correctly represent the TRS dynamics. Similar to the simulation results obtained in the Section 4.4, the ADRC(4) step response presented a faster raising time, and the control signal effort required was larger than for the ADRC(3), as seen in Figure 5.6b. It is due to the ADRC(4) be tuned to produce a more aggressive reaction.

The experimental results of the first group of pure ADRC strategies with a sinusoidal reference are shown in Figure 5.7, which indicates that neither the ADRC(3) nor the ADRC(4) were able to track this time-varying reference, destabilizing the TRS. These experimental results show a TRS instability more noticeable than the one obtained in

Section 4.4. This behavior is a consequence of an increase in the time-delay due to the ESO dynamics and to the accumulation of ripples.

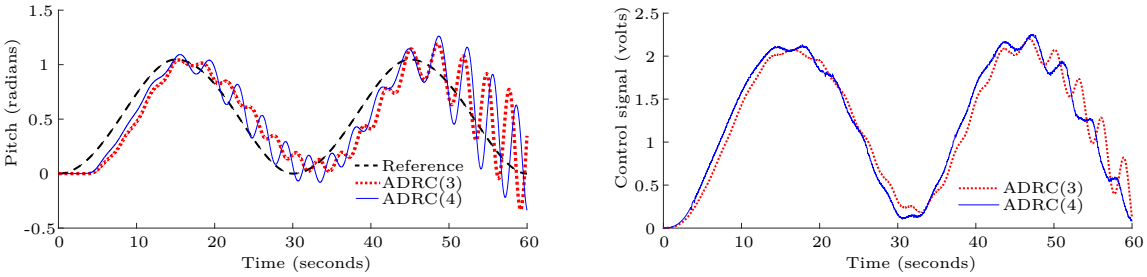

(a) Simulation Results. (b) Control Signal.

Figure 5.7: Experimental results of the first group using a sinusoidal reference.

5.3.2 The Modified ADRC Strategies with Real TRS

The step responses obtained for the second group of modified ADRC strategies are shown in Figure 5.8.

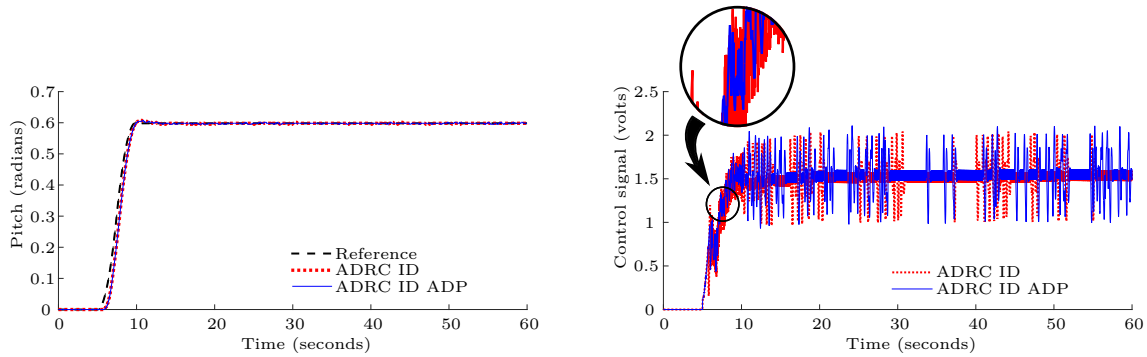

(a) Simulation Results. (b) Control Signal.

Figure 5.8: Step responses of the second group.

Figure 5.8a shows that the modified ADRC produced an excellent step response. Similar to the simulation results obtained in Section 4.4, both control strategies quickly converged to the reference with a non-oscillatory response. Furthermore, the time-delay introduced by the ESO was reduced as a consequence of the dynamical cancellation obtained from the ID scheme. As can be seen in Figure 5.8b, the control signal result shows that the ADRC ID was more aggressive, presenting a higher control effort than the ADRC ID ADP, which corroborates the idea that the ADP decreases the quantized output effect.

The experimental results obtained for the second group of modified ADRCs with a sinusoidal reference are depicted in Figure 5.9, which show that both controllers achieved a good performance, maintaining stable the TRS. Therefore, the control behavior produced by the ADRC with the ID scheme improved the overall results when compared to the

pure ADRCs. Due to the smoothness properties of the algebraic differentiator procedure used in the ESO input, the modified ADRC ID ADP presented less control effort than the ADRC ID, as seen in Figure 5.9a.

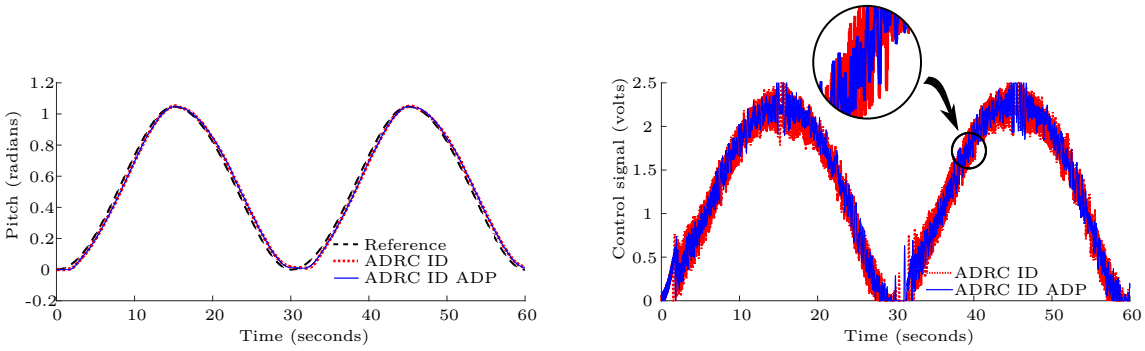

(a) Simulation Results. (b) Control Signal.

Figure 5.9: Experimental results of the second group using a sinusoidal reference.

Similar to Section 4.4, we performed a quantitative analysis of the experimental results obtained by the modified ADRCs in closed-loop with TRS. For this analysis, the sinusoidal reference was chosen as the suitable signal to evaluate the control attitude, and the indexes used were again the IADU, ISE, and ITAE. Table 5.1 summarizes the results.

Performance of the controllers		
Metrics of the control signal		
Metric	ADRC ID	ADRC ID ADP
IADU	781.5698	271.0811
Error between reference and output system		
Metric	ADRC ID	ADRC ID ADP
ISE	0.0571	0.0574
ITAE	51.7209	51.7709

Table 5.1: Performance indexes of the modified ADRCs in the experimental results.

From Table 5.1, one can observe that the experimental results are very close to the simulation results obtained in section 4.4.3. Thus, the successful results obtained for the modified ADRCs are validated through simulation and experimental procedures. The experimental results show that both modified controllers present similar tracking error, but according to the IADU index, the control effort produced by the ADRC ID ADP is significantly smaller when compared to the ADRC ID. Thereby, it is concluded that the ID scheme is able to solve the quantization error of the TRS.

5.3.3 The Modified ADRC ID ADP with Real TRS

With the purpose of evaluating the ability to reject disturbances of the modified ADRC ID ADP during step response, a step disturbance was introduced, as shown in Figure 5.10.

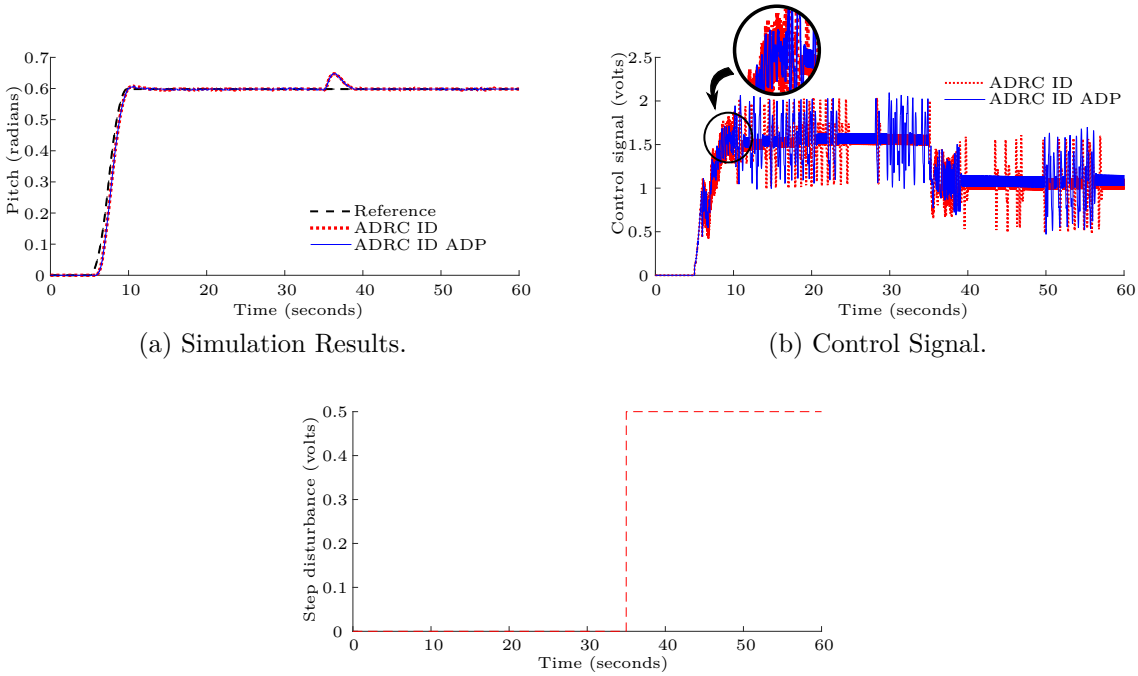

(a) Simulation Results.

(b) Control Signal.

(c) Step Disturbance.

Figure 5.10: Experimental results of the third group using a step reference and a step disturbance.

It can be seen in Figure 5.10a that both modified ADRCs successfully rejected the step disturbance showed in Figure 5.10c, which is introduced in the system, thereafter the controllers kept the TRS stable. These experimental results ensure the good disturbance rejection capability of the modified ADRC. Again, it is shown in Figure 5.10b that the algebraic differentiator procedure is able to reduce the power consumption of the control signal from the ADRC ID ADP when compared to the ADRC ID.

5.4 Final Remarks

This chapter presented the experimental setup used for the TRS, including the main elements of hardware and software used in the experiments. The experimental procedure was described along with the controllers, the parameters and the procedure implemented in the TRS.

Two pure ADRCs and two modified ADRC were used to control the TRS. The experiments were organized in three groups: the first one used the pure ADRCs, first in the step response and then tracking a sinusoidal reference; the second group used the modified ADRCs in the same experimental settings previously defined; and in the third group, a disturbance is introduced in the system to prove the disturbance rejection capacity of the modified ADRCs.

The results obtained in the experiments, through the qualitative and quantitative

analysis, showed that the controller with the lowest tracking error and the lowest control effort was the modified ADRC with ID and ADP. Finally, from the experiments we concluded that the ID scheme in the modified ADRC allows a good performance of the system when tracking a time-varying reference. Also, it was concluded that the ADP subsystem in the modified ADRC allows a decrease in the quantization effect present in the output of the TRS, which indicated that the power consumption of the control signal was improved.

6
Conclusions

This thesis dealt with the nonlinear control study of the model-free technique known as Active Disturbance Rejection Control (ADRC) applied to trajectory tracking problem in pitch motion of the Twin-Rotor System (TRS). The validation of the TRS model, ADRC strategy and modified ADRC strategy was performed in simulation and experimental tests.

The obtained results in this work showed that with the original ADRC formulation it is not possible to control the pitch motion of the TRS in all proposed scenarios. Only for the case of the regulation test the ADRCs pure were able to keep the TRS stable. On the other hand, using the modified ADRCs proposed the control of the pitch motion of the TRS was achieved for all tested scenarios.

6.1 Thesis Overview

The nonlinear system considered in this work was the electromechanical twin-rotor system (TRS), which was configured to have one-degree of freedom in pitch motion and locking up the yaw movement. The mathematical TRS model was obtained by the application of Newton's second law, where the torques caused by weight forces, viscous friction and the propulsion were summed. Quantization errors were included in the model's output, since they appear in the real system, due to the usage of incremental encoders. With the interior-point algorithm, the parameters were found through the minimization of the mean square error between the measured pitch angle of the real TRS and the simulated output of the TRS model.

The Active Disturbance Rejection control (ADRC) proposed by Han (2009) was presented alongside with its main motivation, focused in the development of a new control strategy that replaces the PID control, improved some computational errors and gave robustness to reject disturbances for the control of a set of nonlinear systems. The main ADRC components such as the Transient Profile Generator (TPG), the Extended State Observer (ESO) and the ADRC control law, were detailed in Sections 3.2, 3.3 and 3.4, respectively. To guarantee the stability of the ADRC strategy, the theorems developed by Zheng (2009) were used (where the ESO and ADRC control law convergence is proved, assuming that the nonlinear dynamics is bounded and the second time-derivative of a smooth reference is used in the control law).

Based on the TRS requirements to deal with the electromechanical dynamics of the DC motor and the quantization error, we proposed two additional structures to modify the ADRC. They consist in two differentiator techniques; the first is the algebraic differentiator procedure and the other one is a scheme for the dynamic cancellation, called the inverse dynamics, based on the actuator model of the DC motor and the robust and exact differentiator. With the ADRC and the modified ADRC defined, simulation tests were carried out organized in three groups:

- The first simulation group was carried out using two pure ADRCs, called ADRC(3) and ADRC(4), alongside with the TRS model defined in Chapter 2. The simulation results obtained showed that, for the case were a step reference was used, both controllers could stabilize the TRS, although both included a time-delay in their response. On the other hand, when a sinusoidal reference was used, neither of the controllers were able to keep the TRS stable while tracking the reference;

- In the second group the simulation environment was used to simplify the TRS model, eliminating the DC motor dynamics and using directly the propulsion torque as input system. The pure ADRC(3) and ADRC(4) strategies from the first group were used again. The simulation results obtained showed that the ADRC(4) destabilized the simplified TRS model in both cases of references used (step and sinusoidal signals). On the other hand, the ADRC(3) obtained good simulation results for both trajectories, tracking the reference and stabilizing the simplified TRS model for the two references used;

- Third simulation group used the modified ADRC ID and the modified ADRC ID ADP strategies, which were based on the good results obtained by the ADRC(3) from the second group. In these simulations the complete TRS model was used, which considers the DC motor dynamics, and the modified ADRC strategies, which included the ID scheme. The simulation results obtained from both modified ADRCs showed a good performance tracking the two references used (step and sinusoidal signals).

However, an improvement in power consumption decrease in the control signal was presented by the ADRC ID ADP, which was corroborated by a quantitative analysis.

The tests were carried out in one unit of the TRS that was available to experimentations in the Control Laboratory of the Department of Electronic Engineering at UFMG. The experimental equipment and the necessary software were detailed according to the manual Feedback (2006). The two pure ADRC (ADRC(3) and ADRC(4)) and the two modified ADRC (ADRC ID and ADRC ID ADP) strategies previously proposed where implemented in a PC connected with the TRS equipment, using the MATLAB/Simulink® software. The experimental tests were organized in three groups:

- The first group used the two pure ADRCs in two experimental tests, in which a step response and the tracking of a sinusoidal signals were required. The experimental results obtained showed, as in the simulation test, that both pure ADRCs included a time-delay response. Particularly, the results of an experimental test where the step reference was used, showed that both pure ADRCs were able to stabilize the real TRS. On the other hand, the experimental results of the case where a sinusoidal reference was used, showed that both ADRCs destabilized the real TRS;

- In the second experimental group the two modified ADRCs with two types of references (step and sinusoidal signals) were used. As in the simulation test, the experimental results obtained showed that both modified ADRCs were able to track the two proposed references. However, again an improvement in power consumption in the control signal of the ADRC ID ADP was showed (also corroborated by a quantitative analysis);

- In the third experimental group the disturbance rejection capacity of two modified ADRCs was evaluated. A step reference and step disturbance in the system were used in the tests. The experimental results obtained showed that both controllers were able to reject the step disturbance and keep stable the real TRS. However, the ADRC ID ADP showed improvement decreasing power consumption in the control signal.

Finally, the main contributions obtained in this work are shown below in summary:

- *Development of the TRS model in pitch motion described in state-space equations according to Feedback (2006), parameter identification by the minimization of the mean square error between the measured pitch angle and the simulated output, and validation of the TRS model.* The results obtained in the TRS model validation showed that the chosen TRS parameters and the TRS model could represent the real TRS;

- *Design of two ADRC models for the TRS and the evaluation of the controllers with TRS in simulation and experimental tests.* The simulation and experimental results obtained in the tests showed that the ADRC strategies were able to stabilize the TRS when a step reference was used, but these controllers destabilized the TRS when the tracking of a sinusoidal reference was required;

- *Design of two modified ADRC strategies and the evaluation of the controllers with TRS in simulation and experimental tests.* The simulation and experimental results obtained in the tests showed that the modified ADRC strategies were able to track a time-varying reference for the TRS. It is worth notice that the modified ADRC ID ADP dealt with the quantization error and achieved a decrease in the power consumption in the control signal;

- *During this work an article was published referring to the ADRC modified* (Dulce-Galindo et al., 2016) Dulce-Galindo, J. A., Tôrres, L. A. B., & Raffo, G. V. (2016). A modified active disturbance rejection control applied to the twin-rotor system with output quantization. In *XXI Congresso Brasileiro de Automática* (pp. 3422–3427).

6.2 Future Research

This section describes some possible future works continuing this research line.

- *Theoretic research of the development of a stability prove for the modified ADRC.* Considering that the ADRC stability proof provided by Zheng (2009) does not include the ID and the ADP, the development of the stability proof for the modified ADRC might indicate the ADP parameters that would increase the range of disturbance rejected and also guarantee the stability of the closed-loop system;

- *Development of the modified ADRC for Multiple-Input Multiple-Output (MIMO) systems.* The ADRC strategy has been applied in MIMO nonlinear systems as is shown in Madoński & Herman (2011) and also the modified ADRC might be tested in MIMO systems;

- *Extension of the set of nonlinear systems to which the ADRC can be applied.* Considering that the set of the nonlinear systems defined for the ADRC strategy present full relative degree, the alternative of using coordinate transformations could include some systems that do not have full relative degree;

- *Implementations of the modified ADRC in nonlinear systems in which the ADRC was applied.* The ADRC strategy has been applied in many nonlinear systems, as shown Sira-Ramírez et al. (2011). In this way, the modified ADRC could be implemented in these systems to compare the results;

- *Inclusion of the parametric uncertainties in the TRS for the ADRC formulation.* The ADRC formulation and the choice of the ADRC parameters could be based on a nonlinear system with parametric uncertainties, which increases the robustness of the ADRC;

- *Performance comparison between the modified ADRC and the feedback control based on inverse dynamics.* The proposed modified ADRC breaks the conditions of the complete model-free control but it showed an improvement in its results obtained in comparison with the pure ADRC. A comparative study between the modified ADRC and the a feedback control based on inverse dynamic, which is model-based control strategy, could show more advantages and disadvantages of the modified ADRC.

Bibliography

Aguirre, L. A. (2004). *Introdução à identificação de sistemas–Técnicas lineares e não-lineares aplicadas a sistemas reais*. Editora UFMG.

Bartolini, G., Pisano, A., Punta, E., & Usai, E. (2003). A survey of applications of second-order sliding mode control to mechanical systems. *International Journal of Control*, 76(9-10), 875–892.

Chen, W.-H. (2004). Disturbance observer based control for nonlinear systems. *IEEE/ASME transactions on mechatronics*, 9(4), 706–710.

Chen, W.-H., Ballance, D. J., Gawthrop, P. J., & O'Reilly, J. (2000). A nonlinear disturbance observer for robotic manipulators. *IEEE Transactions on industrial Electronics*, 47(4), 932–938.

Chen, W.-H., Yang, J., Guo, L., & Li, S. (2016). Disturbance-observer-based control and related methods-an overview. *IEEE Transactions on Industrial Electronics*, 63(2), 1083–1095.

Cortés-Romero, J. A., Luviano-Juarez, A., & Sira-Ramírez, H. (2009). Robust GPI controller for trajectory tracking for induction motors. In *2009 IEEE International Conference on Mechatronics* (pp. 1–6).

Davis, P. J. & Rabinowitz, P. (2007). *Methods of numerical integration*. Courier Corporation.

Doyle, J. & Stein, G. (1979). Robustness with observers. *IEEE Transactions on Automatic Control*, 24(4), 607–611.

Dulce-Galindo, J. A., Tôrres, L. A. B., & Raffo, G. V. (2016). A modified active disturbance rejection control applied to the twin-rotor system with output quantization. In *XXI Congresso Brasileiro de Automática* (pp. 3422–3427).

Esfandiari, F. & Khalil, H. K. (1992). Output feedback stabilization of fully linearizable systems. *International Journal of control*, 56(5), 1007–1037.

Feedback (2006). *Twin Rotor MIMO System Control Experiments 33-949S*. Feedback Instruments Ltd., 1 edition.

Fitzgerald, A. E., Kingsley, C., Umans, S. D., & James, B. (2003). *Electric machinery*, volume 5. McGraw-Hill New York.

Fliess, M. & Join, C. (2008). Intelligent PID controllers. In *2008 16th Mediterranean Conference on Control and Automation* (pp. 326–331).

Fliess, M. & Join, C. (2013). Model-free control. *International Journal of Control*, 86(12), 2228–2252.

Fliess, M. & Sira-Ramírez, H. (2003). An algebraic framework for linear identification. *ESAIM: Control, Optimisation and Calculus of Variations*, 9, 151–168.

Fliess, M. & Sira-Ramírez, H. (2004). Control via state estimations of some nonlinear systems. In *IFAC Symposium on Nonlinear Control Systtems (NOLCOS 2004)*.

Gao, Z. (2006). Active disturbance rejection control: a paradigm shift in feedback control system design. In *2006 American control conference* (pp. 7–pp).

Gao, Z. (2015). Active disturbance rejection control: From an enduring idea to an emerging technology. In *2015 10th International Workshop on Robot Motion and Control (RoMoCo)* (pp. 269–282).

Gao, Z., Huang, Y., & Han, J. (2001). An alternative paradigm for control system design. In *Proceedings of the 40th IEEE Conference on Decision and Control, 2001*, volume 5 (pp. 4578–4585).

Gauthier, J. P., Hammouri, H., & Othman, S. (1992). A simple observer for nonlinear systems applications to bioreactors. *IEEE Transactions on automatic control*, 37(6), 875–880.

Gertler, J. J. (1988). Survey of model-based failure detection and isolation in complex plants. *IEEE Control systems magazine*, 8(6), 3–11.

Gorczyca, P., Rosół, M., Turnau, A., Marchewka, D., & Kołek, K. (2013). Model and identification of aerodynamic one rotor system. *Modelowanie inżynierskie*, (49), 12–17.

Han, J. (1989). Control theory: the doctrine of model or the doctrine of control. *System Science and Mathematics*, 9(4), 328–335.

Han, J. (1995). A class of extended state observers for uncertain systems. *Control and decision*, 10(1), 85–88.

Han, J. (2008). Active disturbance rejection control technique-the technique for estimating and compensating the uncertainties. *National Defense Industry Press Beijing, China (in Chinese)*.

Han, J. (2009). From PID to active disturbance rejection control. *IEEE transactions on Industrial Electronics*, 56(3), 900–906.

Huang, Y. & Xue, W. (2014). Active disturbance rejection control: methodology and theoretical analysis. *ISA transactions*, 53(4), 963–976.

Johnson, C. (1968). Optimal control of the linear regulator with constant disturbances. *IEEE Transactions on Automatic Control*, 13(4), 416–421.

Johnson, C. (1970). Further study of the linear regulator with disturbances–The case of vector disturbances satisfying a linear differential equation. *IEEE Transactions on Automatic Control*, 15(2), 222–228.

Johnson, C. (1971). Accommodation of external disturbances in linear regulator and servomechanism problems. *IEEE Transactions on automatic control*, 16(6), 635–644.

Johnson, C. D. (1985). Adaptive controller design using disturbance-accommodation techniques. *International Journal of Control*, 42(1), 193–210.

Johnson, C. D. (2008). Real-time disturbance-observers; origin and evolution of the idea part 1: The early years. In *2008 40th Southeastern Symposium on System Theory (SSST)* (pp. 88–91).

Kelly, R., Llamas, J., & Campa, R. (2000). A measurement procedure for viscous and coulomb friction. *IEEE Transactions on instrumentation and measurement*, 49(4), 857–861.

Khalil, H. & Saberi, A. (1987). Adaptive stabilization of a class of nonlinear systems using high-gain feedback. *IEEE Transactions on Automatic Control*, 32(11), 1031–1035.

Khalil, H. K. (2001). *Nonlinear Systems*. Prentice Hall, third edition.

Khalil, H. K. & Praly, L. (2014). High-gain observers in nonlinear feedback control. *International Journal of Robust and Nonlinear Control*, 24(6), 993–1015.

Khalil, H. K. & Priess, S. (2016). Analysis of the use of low-pass filters with high-gain observers. *IFAC-PapersOnLine*, 49(18), 488–492.

Kirk, D. E. (2012). *Optimal control theory: an introduction*. Courier Corporation.

Le, D., Salas, O., Castaneda, H., & De Leon-Morales, J. (2013). Attitude observer-based robust control for a twin rotor system. *Kybernetika*, 49(5), 809–828.

Lee, H. S. & Tomizuka, M. (1996). Robust motion controller design for high-accuracy positioning systems. *IEEE Transactions on Industrial Electronics*, 43(1), 48–55.

Levant, A. (1998). Robust exact differentiation via sliding mode technique. *Automatica*, 34(3), 379–384.

Li, J., Qi, X., Xia, Y., & Gao, Z. (2016). On asymptotic stability for nonlinear ADRC based control system with application to the ball-beam problem. In *2016 American Control Conference (ACC)* (pp. 4725–4730).

Liberzon, D. (2012). *Calculus of variations and optimal control theory: a concise introduction*. Princeton University Press.

López-Martínez, M. (2005). *Control No Lineal de Sistemas con Dos Rotores Independientes*. PhD thesis, Universidad de Sevilla, Dpto. de Ingeniería de Sistemas y Automática.

Luviano-Juarez, A., Cortés-Romero, J., & Sira-Ramírez, H. (2010). Synchronization of chaotic oscillators by means of generalized proportional integral observers. *International Journal of Bifurcation and Chaos*, 20(05), 1509–1517.

Madoński, R., Gao, Z., & Łakomy, K. (2015). Towards a turnkey solution of industrial control under the active disturbance rejection paradigm. In *2015 54th Annual Conference of the Society of Instrument and Control Engineers of Japan (SICE)* (pp. 616–621).

Madoński, R. & Herman, P. (2011). An experimental verification of ADRC robustness on a cross-coupled aerodynamical system. In *2011 IEEE International Symposium on Industrial Electronics* (pp. 859–863).

Madoński, R., Kordasz, M., & Sauer, P. (2014). Application of a disturbance-rejection controller for robotic-enhanced limb rehabilitation trainings. *ISA transactions*, 53(4), 899–908.

Mboup, M., Join, C., & Fliess, M. (2009). Numerical differentiation with annihilators in noisy environment. *Numerical Algorithms*, 50(4), 439–467.

Mohadjer, M. & Johnson, C. D. (1983). Power system control with disturbance-accommodation. In *The 22nd IEEE Conference on Decision and Control*, volume 22 (pp. 1429–1433).

Mohammad Ridha, T., Moog, C. H., Delaleau, E., Fliess, M., & Join, C. (2015). A variable reference trajectory for model-free glycemia regulation. In *2015 Proceedings of the Conference on Control and its Applications* (pp. 60–67).

Ohishi, K., Ohnishi, K., & Miyachi, K. (1983). Torque-speed regulation of DC motor based on load torque estimation method. In *Unknown Host Publication Title*, volume 2 (pp. 1209–1218).

Olfati-Saber, R. & Shamma, J. S. (2005). Consensus filters for sensor networks and distributed sensor fusion. In *Proceedings of the 44th IEEE Conference on Decision and Control* (pp. 6698–6703).

Prasov, A. A. & Khalil, H. K. (2013). A nonlinear high-gain observer for systems with measurement noise in a feedback control framework. *IEEE Transactions on Automatic Control*, 58(3), 569–580.

Radke, A. & Gao, Z. (2006). A survey of state and disturbance observers for practitioners. In *2006 American Control Conference (ACC)* (pp. 6–pp).

Reger, J. & Jouffroy, J. (2009). On algebraic time-derivative estimation and deadbeat state reconstruction. In *Proceedings of the 48h IEEE Conference on Decision and Control (CDC) held jointly with 2009 28th Chinese Control Conference* (pp. 1740–1745).

Reger, J., Ramírez, H. S., & Fliess, M. (2005). On non-asymptotic observation of nonlinear systems. In *Proceedings of the 44th IEEE Conference on Decision and Control* (pp. 4219–4224).

Rotondo, D., Nejjari, F., & Puig, V. (2013). Quasi-LPV modeling, identification and control of a twin rotor MIMO system. *Control Engineering Practice*, 21(6), 829–846.

Saberi, A. & Sannuti, P. (1990). Observer design for loop transfer recovery and for uncertain dynamical systems. *IEEE Transactions on Automatic Control*, 35(8), 878–897.

Sariyildiz, E. & Ohnishi, K. (2013). A guide to design disturbance observer. *Journal of Dynamic Systems, Measurement, and Control*, 136(2), 021011.

Schrijver, E. & Van Dijk, J. (2002). Disturbance observers for rigid mechanical systems: equivalence, stability, and design. *Journal of Dynamic Systems, Measurement, and Control*, 124(4), 539–548.

Shim, H. & Liberzon, D. (2016). Nonlinear observers robust to measurement disturbances in an ISS sense. *IEEE Transactions on Automatic Control*, 61(1), 48–61.

Shtessel, Y., Edwards, C., Fridman, L., & Levant, A. (2014). *Sliding mode control and observation*. Springer.

Sira-Ramírez, H., Luviano-Jucrez, A., & Corté-Romero, J. (2011). Control lineal robusto de sistemas no lineales diferencialmente planos. *Revista Iberoamericana de Automática e Informática Industrial RIAI*, 8(1), 14–28.

Sira-Ramírez, H., Núñez, C. A., & Visairo, N. (2010). Robust sigma–delta generalised proportional integral observer based control of a buck converter with uncertain loads. *International Journal of Control*, 83(8), 1631–1640.

Slotine, J.-J. & Li, W. (1990). *Applied Nonlinear Control*. Prentice Hall.

Su, Y. X., Duan, B. Y., Zheng, C. H., Zhang, Y., Chen, G., & Mi, J. (2004). Disturbance-rejection high-precision motion control of a stewart platform. *IEEE transactions on control systems technology*, 12(3), 364–374.

Su, Y. X., Zheng, C. H., & Duan, B. Y. (2005). Automatic disturbances rejection controller for precise motion control of permanent-magnet synchronous motors. *IEEE Transactions on Industrial Electronics*, 52(3), 814–823.

Sun, B. & Gao, Z. (2005). A DSP-based active disturbance rejection control design for a 1-kw H-bridge DC-DC power converter. *IEEE Transactions on Industrial Electronics*, 52(5), 1271–1277.

Sun, D. (2007). Comments on active disturbance rejection control. *IEEE Transactions on Industrial Electronics*, 54(6), 3428–3429.

Takahashi, R. & Peres, P. (1999). Unknown input observers for uncertain systems: A unifying approach. *European Journal of Control*, 5(2-4), 261–275.

Tian, G. & Gao, Z. (2009). Benchmark tests of active disturbance rejection control on an industrial motion control platform. In *2009 American Control Conference (ACC)* (pp. 5552–5557).

Tilli, A. & Montanari, M. (2001). A low-noise estimator of angular speed and acceleration from shaft encoder measurement. *Automatika*, 42(3-4), 169–176.

Tornambe, A. (1989). Use of asymptotic observers having-high-gains in the state and parameter estimation. In *Proceedings of the 28th IEEE Conference on Decision and Control* (pp. 1791–1794).

Umeno, T. & Hori, Y. (1991). Robust speed control of DC servomotors using modern two degrees-of-freedom controller design. *IEEE Transactions on Industrial Electronics*, 38(5), 363–368.

Vivas Venegas, C. (2004). *Control óptimo y Robusto H_∞ de Sistemas No Lineales. Aplicaciones a Sistemas Electromecánicos.* PhD thesis, Universidad de Sevilla, Dpto. de Ingeniería de Sistemas y Automática.

Xie, H., Song, K., Yang, S., Tatsumi, J., Zheng, Q., Zhang, H., & Gao, Z. (2016). On decoupling control of the VGT-EGR system in diesel engines: A new framework. *IEEE Transactions on Control Systems Technology*, 24(5), 1788–1796.

Xue, W. & Huang, Y. (2011). Comparison of the DOB based control, a special kind of PID control and ADRC. In *2011 American Control Conference (ACC)* (pp. 4373–4379).

Yoo, D., Yau, S.-T., & Gao, Z. (2007). Optimal fast tracking observer bandwidth of the linear extended state observer. *International Journal of Control*, 80(1), 102–111.

Zehetner, J., Reger, J., & Horn, M. (2007). A derivative estimation toolbox based on algebraic methods – theory and practice. *Proceedings of the IEEE International Conference on Control Applications*, (5), 331–336.

Zhao, S. & Gao, Z. (2013). An active disturbance rejection based approach to vibration suppression in two-inertia systems. *Asian Journal of Control*, 15(2), 350–362.

Zheng, Q. (2009). *On active disturbance rejection control: stability analysis and applications in disturbance decoupling control*. PhD thesis, Cleveland State University.

Zheng, Q., Gao, L. Q., & Gao, Z. (2007). On stability analysis of active disturbance rejection control for nonlinear time-varying plants with unknown dynamics. In *2007 46th IEEE Conference on Decision and Control* (pp. 3501–3506).

Zheng, Q. & Gao, Z. (2012). An energy saving, factory-validated disturbance decoupling control design for extrusion processes. In *Proceedings of the 10th World Congress on Intelligent Control and Automation* (pp. 2891–2896).

Zheng, Q. & Gao, Z. (2014). Predictive active disturbance rejection control for processes with time delay. *ISA transactions*, 53(4), 873–881.

Zheng, Q. & Gao, Z. (2016). On active disturbance rejection for systems with input time-delays and unknown dynamics. In *2016 American Control Conference (ACC)* (pp. 95–100).